Title
KINETICS OF THE DISSOLUTION AND DIFFUSION OF THE OXIDES OR IRON IN SODIUM DISILICATE GLASS

Author
Borom, Marcus Preston.

Publication Date
1965-08-04

UCRL-16232

University of California

Ernest O. Lawrence Radiation Laboratory

KINETICS OF THE DISSOLUTION AND DIFFUSION OF THE OXIDES OF IRON IN SODIUM DISILICATE GLASS

Berkeley, California

DISCLAIMER

UCRL-16232

Research and Development

UNIVERSITY OF CALIFORNIA

Lawrence Radiation Laboratory
Berkeley, California

AEC Contract No. W-7405-eng-48

KINETICS OF THE DISSOLUTION AND DIFFUSION OF THE OXIDES OF IRON IN SODIUM DISILICATE GLASS

Marcus Preston Borom
(Ph. D. Thesis)

August 4, 1965

KINETICS OF THE DISSOLUTION AND DIFFUSION OF THE OXIDES OF IRON IN SODIUM DISILICATE GLASS

Contents

I. INTRODUCTION

The dissolution of a refractory oxide by a molten slag or glass at elevated temperatures is a process frequently encountered in ceramic systems. The importance of understanding the kinetics of such phenomena becomes apparent when one considers the application of this knowledge to specific systems and problems--for example, the formation and homogenization of a glass from various materials, many of which are solids at the smelting temperature, or the sintering or densification of solid phases in the presence of a liquid phase. The specific example covered in this study, the dissolution of the oxides of iron by a model glass, has its application in the realm of glass-metal seal and enamel technology.

The problem of the development of adherence between dissimilar materials has been one of perennial interest among those engaged in the application of a glass to a metal surface. Numerous theories have been advanced regarding adherence of glass to metal. These range from a description of a strictly mechanical interlocking of the two materials to the theory of the development of a chemical bond at the interface. Some of these theories are covered in a recent review article by Eitel.[1] Concurrent studies at the University of California[2] and at the Battelle Memorial Institute[3] are responsible for the postulation of the theory of chemical bounding occurring at glass-metal interfaces.

In any heterogeneous mixture of nonequilibrium phases, reactions occur if the thermodynamics are favorable, and, if the kinetics are favorable, equilibrium compositions are immediately established at the interfaces and the entire system tends toward these equilibrium compositions through diffusional processes. This reasoning has been the basis of a recent article by Pask and Borom[4] on the physical chemistry of glass-metal interfaces. The complexity of the phenomena involved in attaining and maintaining these equilibrium compositions at the interface of a commercial enamel and iron has been treated in a semiquantitative manner by Borom and Pask.[5] Similar work of a more quantitative nature with a model system[6] describes chemical reactions involving the uphill diffusion of sodium ions and the precipitation of metallic phases from the bulk glass.

The firing techniques generally used in the enameling industry result in the formation of an oxide layer on the base metal prior to the fusing of the glass coating. The dissolution of this oxide layer, if diffusion-controlled, results in the establishment of a composition at the interface which is an equilibrium phase with respect to the base metal itself. This study is concerned only with investigation of the interaction between a glass and the oxides of iron. The complications involved in the maintenance of equilibrium upon complete solution of the oxide and contact of the base metal by the glass have been treated in part in an earlier study.[7]

Studies of ionic diffusion in glass have been numerous, but they have dealt primarily with the determination of the self-diffusion coefficients of the more commonly occurring ions in glass. A review article has been written on this subject by Williams.[8] Iron is admittedly not a normal constituent in glass compositions; however, the lack of information on the diffusion of iron in glass is quite surprising when one considers the wide-spread use of glass as a protective or decorative coating for iron and iron alloys. Values for the self-diffusion coefficient of iron and an activation energy for diffusion have been reported by Yang, Chien, and Derge[9] for an iron silicate melt in the temperature range 1250 to 1304°C. A value for the diffusion coefficient of ferrous iron in sodium disilicate glass of approximately 4×10^{-7} at 1100°C, calculated from chemical equilibrium studies, has been reported by Johnston.[10] Tashiro[11] has reported "diffusion velocities" for FeO in an enamel and a diffusion activation energy of 53 kcal/mole.

Studies of the dissolution of refractory oxides by their slags in the system $CaO-Al_2O_3-SiO_2$ have been conducted by Kingery et al.,[12,13] and the dissolution was found to be diffusion-controlled. Mathematics for the interpretation of the concentration distributions resulting from dissolution in ternary oxide systems in terms of the self-diffusion coefficients of the cations have been proposed by Oishi, Cooper, and Kingery.[14] These mathematical relationships have so far been used only to calculate the ratio of diffusivities and have not been applied to a quantitative calculation of the diffusivities of the respective components based on their concentration distributions. The mathematical

relationships referred to here are based on Oishi's description[15] of the flux-density equations for ternary diffusion by extending Darken's analysis for binary diffusion to include three components. Oishi[16] has given the solution of these diffusion equations in closed form, and has demonstrated the validity of the mathematics through empirical observations.[17] His experiments involved the study of diffusion couples of glasses in the $CaO-Al_2O_3-SiO_2$ system and a comparison of the observed concentration distribution with that predicted on the basis of the derived mathematics and the known values of the self-diffusion coefficients.

The purpose of the study presented here is to determine if the dissolution of the oxides of iron by sodium disilicate glass is controlled by diffusion in the molten glass and, if so, to analyze the diffusion phenomena in terms of the equations for ternary diffusion. Even though the parameters have been reduced here by the choice of a glass with only two oxide components, the results and techniques described should have a general application in the technologies of enameling and of glass-metal sealing. For instance, if one knows or can easily measure the rate at which an oxide, formed on a base metal, is dissolved by an applied glass coating, a firing cycle can be designed to optimize the conditions for the formation of a chemical bond at the interface.

II. THEORY

Diffusion is a process by which chemical units distribute themselves in order to establish and maintain homogeneity or chemical equilibrium in a system. Diffusion may take place without a resultant transfer of mass (self-diffusion), or with a transfer of mass. In the former case the atomic motion is that which occurs in a homogeneous material by a purely random-walk process. Here the motion can be followed only by the use of some suitable tracer-atom technique. The latter case actually involves concentration or, more exactly, chemical potential gradients within the system as the driving force for the motion of the various chemical units, and is the case to be considered in this study. For these conditions the motion may be followed by direct chemical analysis of compositions along the diffusion direction.

The bases for all diffusion theory are Fick's first and second laws, which, stated mathematically, are

$$J_i = -D \frac{\delta c_i}{\delta x} \tag{1}$$

and

$$\frac{\delta c_i}{\delta t} = D \frac{\delta^2 c_i}{\delta x^2}, \tag{2}$$

where J_i is the flux of species i passing a plane of unit area per unit of time, c_i is the concentration of species i per unit volume of material, t is the time, and D is a constant of proportionality termed the diffusion coefficient or the diffusivity, and generally has the units of cm^2/sec. If there is no mass transfer, D is the self-diffusion coefficient of species i; when mass transfer is involved, D is referred to as an interdiffusivity and requires further description in order to be expressed in terms of the diffusivities of the individual species.

The units generally used, as indicated above, are centimeters, seconds, and any convenient concentration unit just as long as it is expressed per unit of volume. Weight percent is often an acceptable concentration unit, since the density factor appears in the solution to the diffusion equation in such a fashion that it is self-canceling; however, in systems in which the density varies appreciably along the concentration gradient, weight percent figures must be individually corrected for these variations and expressed in terms of weight per unit volume to be exact.

Numerous texts[18-20] are available that discuss diffusion theory in detail and give solutions to the differential equations for diffusion for specific initial and boundary conditions. For example, for binary diffusion of species i into a semi-infinite medium in which the concentration of species i is maintained constant at the surface at which it is introduced, a solution of the diffusion equations is given by Crank[18] as

$$M_t = 2C_s (Dt/\pi)^{1/2} , \tag{3}$$

where M_t is the total amount of species i introduced into the host material in the time t, C_s is the surface concentration of species i, and D is the apparent diffusion coefficient or the interdiffusivity. It is apparent that D could be obtained from the slope of a plot of $(M_t/C_s)^2$ vs t.

In the foregoing discussion, D has been treated as being a constant independent of concentration, when in actuality this is seldom true over more than a limited composition range. For the more general case Fick's second law must be written as

$$\frac{\delta c}{\delta t} = \frac{\delta}{\delta x} \left(D \frac{\delta c}{\delta x} \right) . \tag{4}$$

A solution for this general case is given by Boltzmann's approach[21] as

$$D_{c=c_1} = -\frac{1}{2t} \frac{dx}{dc} \int_0^{c=c_1} x \, dc , \tag{5}$$

provided that the following conditions are met:

(a) the process is diffusion-controlled, i.e., $x_{c=c_1} = kt^{1/2}$;

(b) $x = 0$ is defined by $\int_0^{c=c_0} x \, dc = 0$;

(c) at $t = 0$, $c_i = 0$ for $x > 0$,
$c_i = c_0$ for $x < 0$.

For ternary dissolution in which a solid component is dissolved by a liquid composed of the other two components, and the process is controlled by diffusion in the liquid phase, Oishi et al.[14] have developed, for the flux density of the dissolving or solute species, the relationship

$$J_3 = -\left[\frac{N_1 + N_2}{(N_1 D_2 + N_2 D_1)} (N_1 D_2 D_3 + N_2 D_3 D_1 + N_3 D_1 D_2) \right] \frac{dc_3}{dx} , \tag{6}$$

where the subscripts 1 and 2 refer to the solvent species and subscript 3 refers to the solute species, and J, N, D, c, and x are respectively the flux density, the mole fraction, the self-diffusion coefficient, the mole concentration, and the diffusion distance. The mole concentration gradient is related to the weight percent gradient by the relation

$$\frac{dc}{dx} = \frac{d(\rho W/M)}{dx}, \tag{7}$$

where M is the molecular weight, ρ the density, and W the weight percent. Equation (6) is merely a statement of Fick's first law in terms of the particular case in which the portion in brackets, which is concentration-dependent, is the apparent diffusion coefficient or the interdiffusion coefficient for the solute species. This bracketed term then should be determinable by means of Eq. (5). A more detailed interpretation of this term depends on what additional data may be gained regarding the relative magnitudes of the individual diffusivities.

The temperature dependence of the diffusivity is usually given by the relation

$$D = D_0 e^{-\Delta H/RT}, \tag{8}$$

where R is the gas constant, T the absolute temperature, ΔH the enthalpy of activation, and D_0 the pre-exponential constant, which contains the entropy of activation as $e^{\Delta S/R}$. The enthalpy of activation can be obtained from the slope of a plot of log D vs 1/T, and an insight can be gained into the mechanism of the diffusion process from the obtained value of ΔH.

III. EXPERIMENTAL WORK

A. Preparation of Diffusion Couple

1. Glass

Degassed sodium disilicate glass rod approximately 5/8 in. in diameter was prepared by Corning Glass Works at their research laboratories in Corning, New York. The glass was vacuum-smelted in a platinum container at 1480°C and held at 0.015 torr for 2 h before the cane was drawn under an argon atmosphere. The glass contained 0.005% Cu as the only reported impurity. The composition of the glass as determined in the laboratories at the University of California is by weight 67.5% SiO_2, 32.5% Na_2O. Three-quarter-inch lengths were cut from the rod to serve as diffusion specimens. The ends of the glass specimens were polished through a set of dry polishing papers and given a light polish on a diamond lap wheel. Just prior to a diffusion anneal the glass cylinders were washed in acetone and dried.

2. Substrate Material

The preparation of polycrystalline disks of wüstite was accomplished as follows: Chemically pure (reagent grade) Fe_2O_3 Baker & Adamson powder was heated in vacuum in an alumina crucible for 4 h at temperatures between 1100 and 1200°C to permit decomposition to Fe_3O_4. The success of the decomposition was verified by x-ray diffraction. Powdered iron was mixed with the powdered Fe_3O_4 in an amount to produce stoichiometric FeO on reaction. Since wüstite (ferrous oxide) is nonstoichiometric, this procedure assured an excess of iron for the reaction and set the nonstoichiometry on the iron-rich side of wüstite. The powdered iron-magnetite mixture was mechanically mixed and placed in a 5/8-in. o.d. by 5-in.-high cylinder made from 25-gauge Armco iron. The loaded cylinder was placed inside a porous alumina crucible which was then inserted into a graphite susceptor. This unit was placed in an induction-heated vacuum furnace, which was evacuated to 1×10^{-4} torr. The powdered mixture was heated to 1410°C over a period of approximately 30 min with the pressure maintained at 10^{-4} torr. At 1410°C melting was obviously occurring. The melting point of iron-rich wüstite is given by Darken and Gurry[22] as 1371°C. The sample was held for 30 min at 1410°C, allowed to solidify

for 10 min at 1350°, and then cooled rapidly to room temperature by shutting off the power and flushing with helium after the susceptor had dropped below red heat. Sections approximately 1/16 in. thick were cut from the cylinder, giving a polycrystalline iron oxide disk surrounded by an iron ring. This iron ring along with the bits of excess iron in the oxide served as markers of the original interface in the diffusion anneals. The oxide crystals were large and radially oriented. X-ray diffraction powder patterns showed the disks to contain wüstite as the only oxide of iron. Electron microprobe analysis of the disks indicated 77 wt % Fe, which corresponds to the iron-rich composition of wüstite. The advantage of this composition is that it is not subject to the rapid transformation to wüstite plus magnetite which occurs above 560°C for the more iron-deficient compositions. The presence of magnetite in the wüstite substrate would obviously complicate interpretation of the diffusion data. Any magnetite which might form as a result of the sluggish transformation to α-iron plus magnetite below 560°C would simply convert to wüstite on heating in the case of the iron-rich composition.

The oxide disks were polished through a set of dry polishing papers and given a final high metallurgical polish on a lap wheel with 2-μ diamond.

Naturally occurring magnetite from the Marble Mountains, San Bernardino, California, was used for the Fe_3O_4 substrate material. Dodecahedral crystals of magnetite up to 5/8 in. across occurred on the surface of the polycrystalline mass, and sections through these larger crystals were used in the diffusion studies. The polycrystalline bulk contained considerable amounts of visible impurities, but these regions were avoided as much as possible. The selected sections were prepared for the diffusion anneals in the same fashion as the wüstite. The only chemical analysis of this material was conducted with the electron probe, which indicated that the samples chosen for diffusion studies were homogeneous and possessed an iron content corresponding to magnetite.

Naturally occurring single-crystal stock of hematite from Rio Marina, Island of Elba, Italy, was used as the Fe_2O_3 substrate material. Previous samples from this source analyzed by the U. S. Bureau of Mines, Berkeley, California, proved to be of high purity. Sample preparation was identical to that of the other substrate materials.

Both the magnetite and the hematite specimens were obtained from Minerals Unlimited of Berkeley, California.

3. Construction of the Diffusion Cell

The diffusion couple, consisting of a 1/2- to 3/4-in. section of the degassed sodium disilicate glass rod and the appropriate substrate material, was placed substrate first into a recrystallized alumina crucible approximately 1 in. high and 5/8 in. i.d. (Coors catalog No. CN-5). The alumina crucible was placed in a sample bucket made of either graphite (wüstite diffusion anneals) or platinum mesh (magnetite and hematite diffusion anneals) fitted with a Pt/Pt-10% Rh thermocouple to monitor the sample temperature. A schematic diagram of the graphite sample bucket is shown in Fig. 1.

Platinum has been shown by several authors[10,23] to be an unsatisfactory container material for quantitative studies of iron silicate melts because of reduction of the iron and formation of an alloy with the platinum. Contamination of these melts was also expected with the use of alumina crucibles,[10] but it was assumed not to be extensive in the temperature range of these experiments. Edge effects on the diffusion profile due to contamination by the crucible material were eliminated, however, by the selection of an appropriate crucible diameter.

B. Diffusion Anneals

1. Furnace Construction

A vertical resistance-wound furnace was utilized which was capable of operating under conditions of either vacuum or controlled atmosphere. The diffusion cell could be raised or lowered in the furnace without affecting the furnace atmosphere by means of a refractory porcelain four-hole thermocouple tube which moved freely through a Wilson-type vacuum seal. The porcelain tube served both as a support rod for the diffusion cell and as a conduit for the thermocouple leads. The vertical temperature gradient in the furnace was adjusted to less than ± 1°C over the length of the diffusion cell by means of external taps and rheostats. A schematic diagram of the furnace is shown in Fig. 2, and typical furnace temperature and power gradients are shown in Fig. 3.

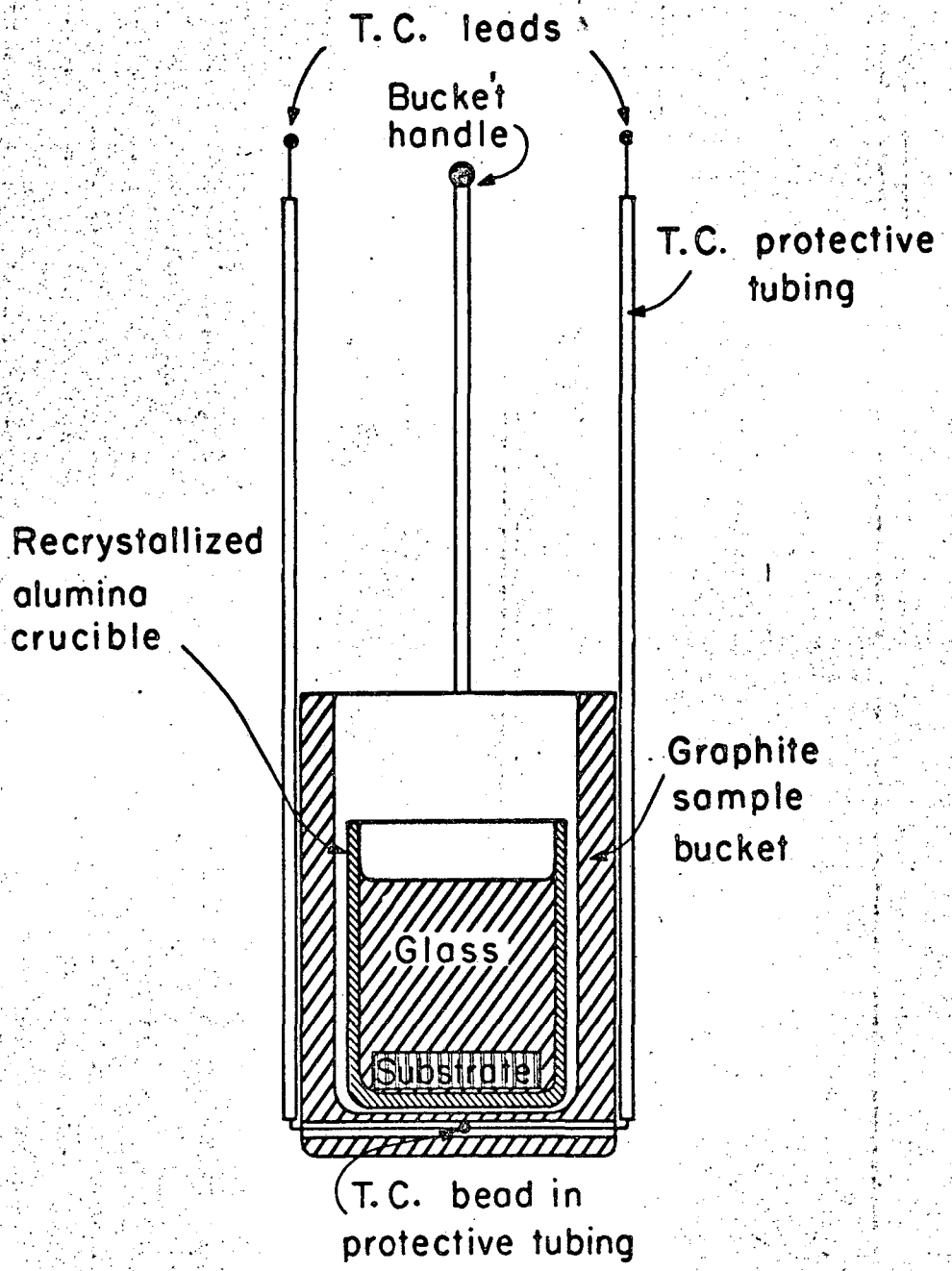

Fig. 1. Schematic of diffusion cell.

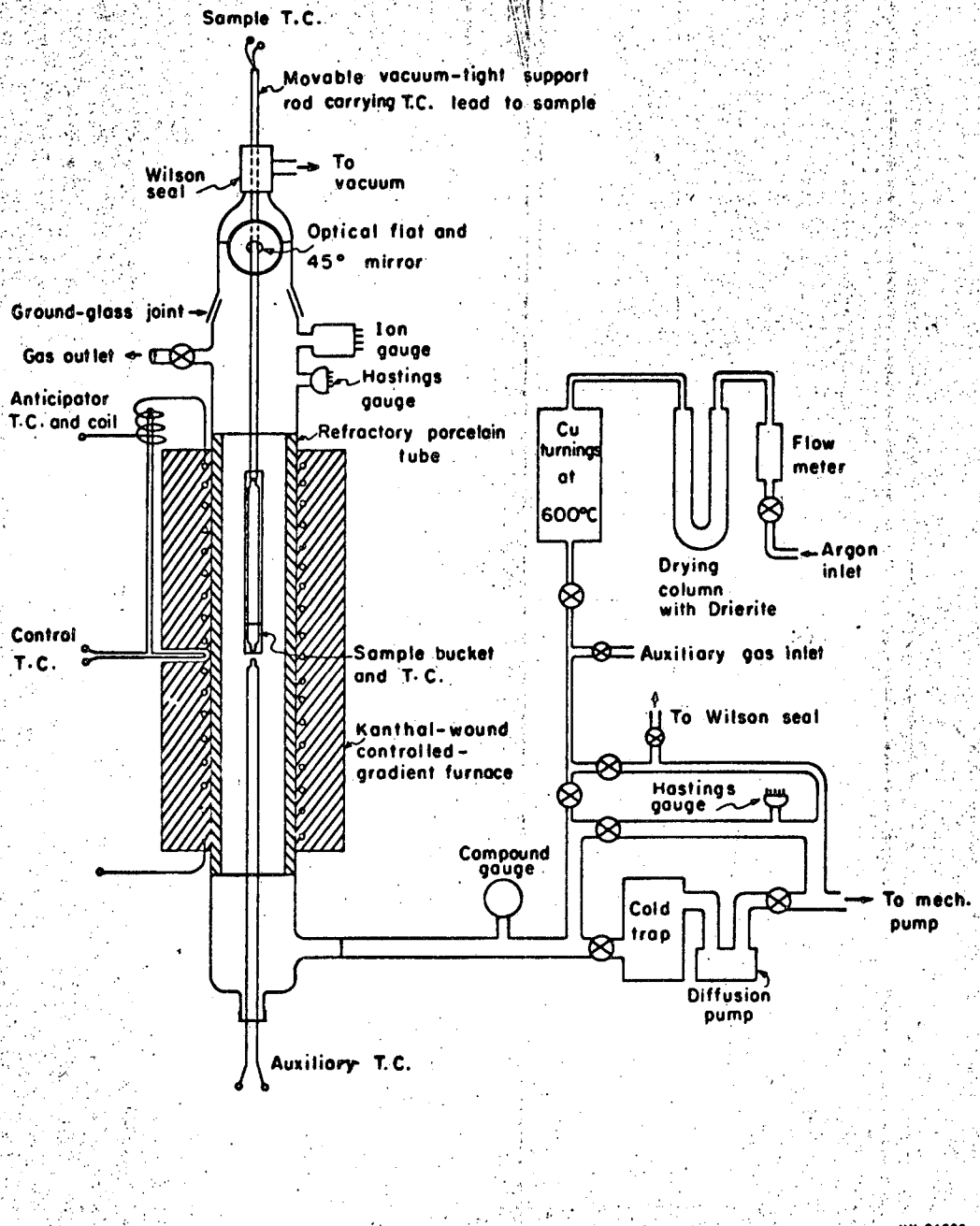

Fig. 2. Schematic diagram of diffusion furnace.

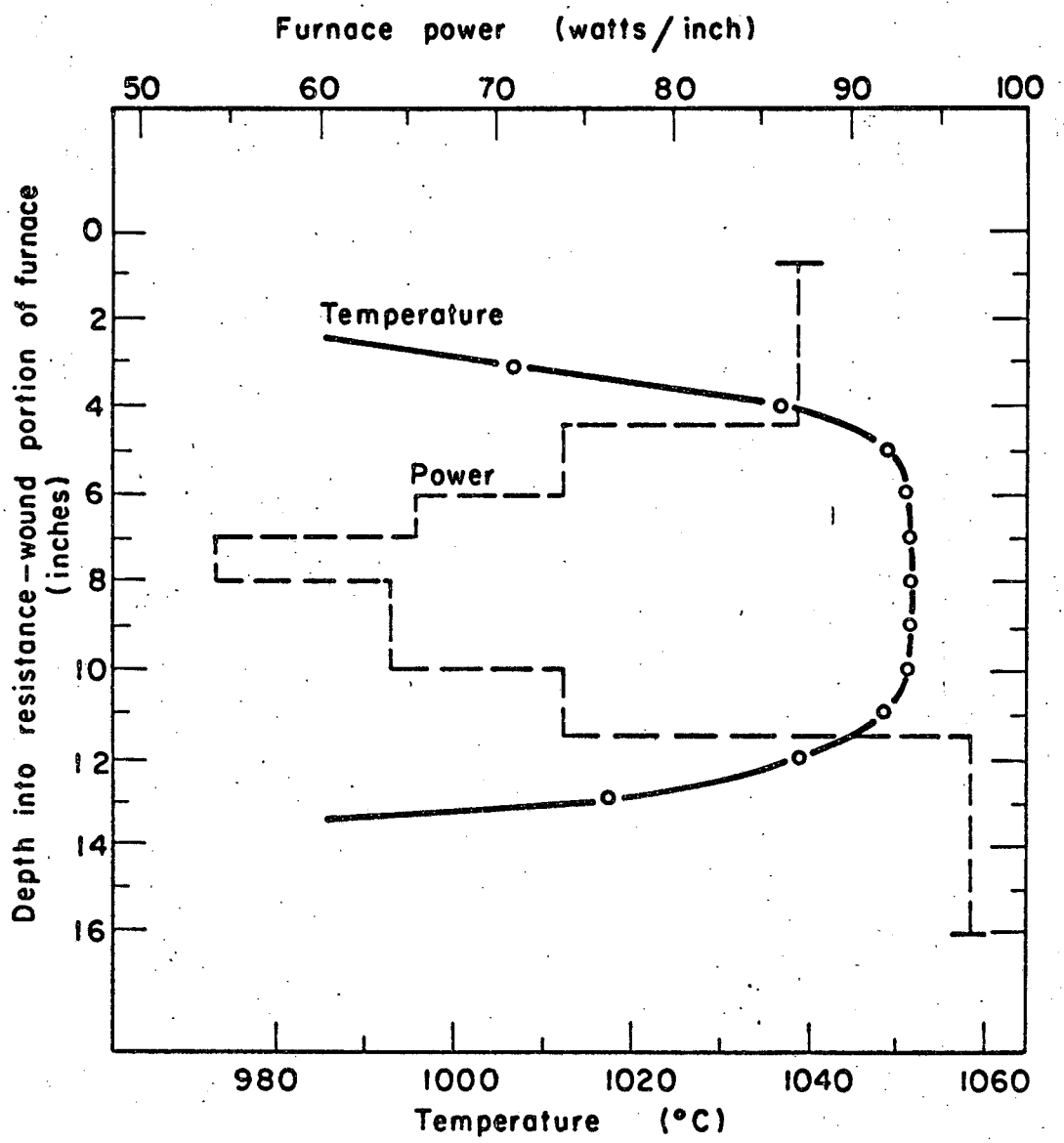

Fig. 3. Plot of typical furnace temperature and power gradients.

2. Experimental Procedure

For the wüstite diffusion anneals the diffusion cell was outgassed in the cold zone of the furnace for up to 24 h to a pressure of 10^{-5} torr or less before being lowered into the hot zone. The sample temperature was monitored by the Pt/Pt-10% Rh thermocouple mounted in the sample bucket, and the temperature was automatically recorded on a Leeds & Northrup Adjustable Span Adjustable Range (ASAR) Speedomax recorder. This technique permitted further outgassing of the cell below 400°C. From this point the cell was completely lowered into the furnace, passing through the softening point of the glass (598°C) and reaching the test temperature within 5 min. The furnace pressures as the sample approached the test temperature ranged from 10^{-4} to 10^{-3} torr. A flowing atmosphere of dried and purified argon was introduced into the furnace as the sample temperature reached within 50°C of the test temperature. It was assumed that prior to this point the wüstite had been wet by the glass and the interface sealed under as low a partial pressure of oxygen as possible. The diffusion anneal was conducted under 1 atm of flowing argon to minimize (a) the decomposition of the glass through the spontaneous loss of sodium, (b) any possible entry of atmospheric oxygen into the furnace, and (c) convection that might arise from the evolution of any entrapped gas at the interface or within the bulk materials.

Temperature variations of the sample during the diffusion anneal were indicated on the Leeds & Northrup ASAR Speedomax strip chart recorder with the full-scale sensitivity set at 2 mV and adjusted to the range of the diffusion temperature. Control was maintained with ± 1 to 4°C. The temperature range covered during the experiments was from 900 to 1100°C in increments of 50°. This range was bounded by crystallization of the glass between 800 and 900°C and by furnace limitations above 1100°C.

Upon conclusion of the diffusion run, the sample was withdrawn and allowed to cool rapidly to just above the annealing point (452°C) of the glass. Approximately 15 min was allowed for the sample to pass through the annealing point, after which the sample was withdrawn to the cold portion of the furnace and allowed to cool to room temperature.

The magnetite diffusion anneals were conducted in a similar fashion, with the exception that the atmosphere from beginning to end

was static argon saturated with water vapor at 25°C.

The hematite diffusion anneals were conducted entirely in a static air atmosphere.

Upon conclusion of the diffusion anneal, the alumina crucible containing the diffusion couple was mounted in clear casting resin and a cross section of the diffusion zone perpendicular to the glass-substrate interface was removed from the center of the crucible. This cross section was remounted in casting resin so as to expose the length of the diffusion path for analysis. The cross section was polished down through a set of emery papers and finished to a high metallurgical polish on a lap wheel containing 2-μ diamond. After the surface of the sample had been coated with vapor-deposited carbon to make it conductive, it was subjected to electron microprobe analysis.

C. Electron Microprobe Analysis

The electron microprobe is essentially an x-ray tube that uses the sample in question as the target material. A finely focused electron beam bombards the sample and fluorescent x rays are produced. The characteristic radiation from the particular element being analyzed is resolved by a proper positioning of a diffracting crystal, and the intensity of the radiation is measured with a suitable counter. The position of the sample in relation to the electron beam can be stepwise or continuously changed in either the X or Y direction by means of a manually or motor-driven gear mechanism.

An Applied Research Laboratories electron probe utilized in these studies is capable of simultaneous analysis of Na, Si, and Fe K-alpha radiation. The individual radiation intensities of these three elements as total counts per selected integration time are collected on scalers and recorded by an automatic print-out device. The technique for the analysis of the diffusion profiles or concentration distributions of the three elements in the samples was to take an integrated count for 20 sec at a known distance from the glass-substrate interface, advance a given distance in microns, take another count, and repeat this procedure until a sufficient number of points (between 30 and 40) had been collected to construct a smooth curve.

The fact that a small-diameter (e. g., 2 μ) beam of electrons is impinging directly on the specimen subjects it to a much higher stage loading (watts/unit area) and consequently a much greater tendency for surface damage than in the case of ordinary x-ray fluorescent analysis. This tendency is augmented for intrinsically nonconducting sodium-bearing glasses. An example of the effect that surface damage can have on the count rate is shown graphically in Fig. 4. For this illustration the electron beam was held on the same spot and counts were accumulated over 2-sec intervals. In the sodium disilicate glass, there is a rapid increase in the Na count rate and a decrease in the Si count rate. The presence of iron in the glass appears to stabilize the specimen against this severe effect of surface damage. This figure is admitted only in evidence of the analytical difficulties encountered, and no attempt will be made at a specific explanation of these phenomena.

In order to evaluate the effect of surface damage and to calibrate the probe for quantitative work, 25 standard compositions were prepared in each of the two ternary systems, $FeO-Na_2O-SiO_2$ and $Fe_2O_3-Na_2O-SiO_2$. The raw materials consisted of iron-rich wüstite powder, prepared by K. K. Kelley of the U. S. Bureau of Mines, and reagent-grade hematite, sodium bicarbonate, and silicic acid. One-gram batches were mechanically mixed in plastic containers, sintered at 800°C for 1 h, remixed and sintered two more times, fused above 1100°C in platinum crucibles, crushed and mixed, and re-fused twice, all to insure homogeneity. Heatings were conducted in air for the hematite series and in argon and vacuum for the wüstite series. Twenty-two of the 50 standards were chemically analyzed in the analytical laboratories of the Lawrence Radiation Laboratory and of the Philadelphia Quartz Co. It was found that considerable loss of soda had occurred during the preparation of the standard specimens.

The standard specimens were all mounted in four sample holders and prepared for electron microprobe analysis. It was found that consistent results and smooth calibration curves could be obtained only if the samples were scanned at the fastest speed available (96 μ/min) and if the carbon coating was adequately conductive to minimize surface damage. The thickness of the carbon coating was only visually estimated, but its effectiveness was always checked by compairing the sample current on the critical composition (the undiffused sodium

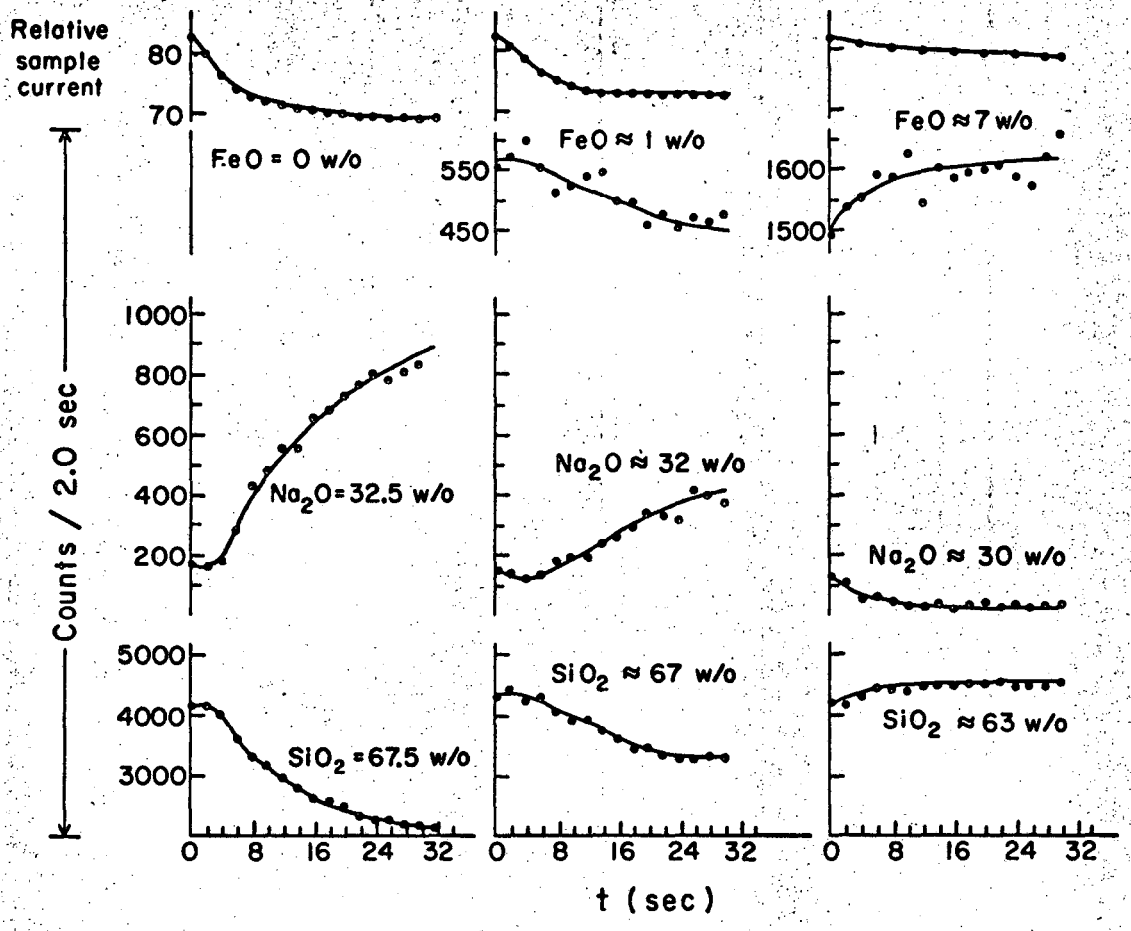

Fig. 4. Electron microprobe data showing the effect of surface damage on the count rate for three glass compositions.

disilicate glass of the test specimens) with the sample current on a stable olivine standard of slightly higher average atomic number. The probe conditions decided upon reduced the Na counts to figures of only semiquantitative value; however, an accuracy of ± 1 to 2% in the Fe and Si analyses justified the determination of Na by difference when the components were expressed as oxide weight percent. (Probe conditions: 15 kV, 0.03 μA, heavy carbon coating, scan parallel to the interface, and integrate count for 20 sec.) The resulting calibration curves agreed with the general trends predicted by calculations based on the best known mass-absorption coefficient data[24] for the elements in question. The SiO_2 calibration curve applied to both the hematite and the wüstite series, and it was found that the Fe calibration curve was directly proportional to the weight percent Fe present and could be adjusted for analysis of either wüstite, magnetite, or hematite compositions by the appropriate weight percentage correction factor. These curves took into account the effects on the count rate due to absorption, secondary fluorescence, background, and variations in the average atomic number of the compositions. No dead-time correction was necessary.

IV. RESULTS

A. Definitions

Before the results are analyzed, the definition of several terms is in order. The data gained from the electron microprobe analysis of the diffusion couples are plotted on coordinates of concentration units vs distance. Such plots are referred to interchangeably as concentration distributions, concentration profiles, or diffusion profiles. All the glass compositions shown by a concentration distribution at a particular temperature may be transferred to a single smooth curve on a triaxial composition diagram. This latter curve is referred to as the concentration path. Such a plot gives no information regarding the concentration vs distance coordinates within the diffusion couple; however, the same concentration path applies for all diffusion times at the temperature of its determination.[16]

B. Diffusion Profiles

The times and temperatures of the various diffusion anneals along with some calculated results are given in Table I. The diffusion profiles for each of the diffusion anneals as determined by microprobe analysis were plotted as weight percent oxide vs distance. A typical profile is shown in Fig. 5 along with a plot of the changing O/Si ratio within the diffusion zone. The O/Si ratio was calculated by converting the weight percent figures into atomic percent and making the appropriate division. Plots of the concentration paths determined from the diffusion profiles of each of the oxides of iron are given in Fig. 6.

The total amount of oxide introduced into the glass by diffusion, M_t, was calculated by determining the area under the iron oxide diffusion profile by weighing the appropriate area of graph paper. These figures are given in Table I. The apparent diffusion coefficients for wüstite were determined from the plots of M_t^2 vs t shown in Fig. 7. Since diffusion profiles for the other oxides of iron were determined at only one time at each temperature, it was necessary to determine the apparent diffusion coefficients by the above method on the basis of a straight line drawn through only one experimental point at each

Table I. Experimental conditions and some calculated results.

Sample number	Temperature (°C)	Time (sec) × 10^{-3}	C_s (wt % Fe Oxide)	Mt (wt % cm)	Dissolved oxide (Microns)		Calc. density of wüstite (g/cm^3)
					Calc.[a]	Measured	
Substrate material: wüstite							
A_0 - 1	901 ± 1	18.0	39.0	1.23	64	75	4.8
2	6 ± 1	36.0		2.00	104	125	4.8
3	1 ± 1	77.4		2.43	126	150	4.8
4	9 ± 3	180.0		3.85	200	215	5.3
B_0 - 1	949 ± 1	18.0	41.0	1.86	96	115	4.8
2	50 ± 1	36.0		2.23	115	130	5.1
3	49 ± 1	81.9		2.86	148	190	4.4
4	48 ± 1	144.0		3.67	190	190	5.7
C_0 - 1	995 ± 2	18.0	42.0	2.24	117		
2	1005 ± 4	36.0		3.14	165		
3	1008 ± 3	72.0		3.99	208		
D_0 - 1	1045 ± 2	18.0	46.0	3.35	176		
2	50 ± 2	36.0		4.28	225		
3	49 ± 3	72.3		5.72	302		
E_0 - 1	1105 ± 2	7.2	53.5	3.11	169		
2	1097 ± 2	18.0		4.03	219		
3	1102 ± 1	36.0		5.27	287		
Substrate material: magnetite							
A - O_4	898 ± 1	18.0	36.0	0.380	20		
B	944 ± 1	36.0	38.0	0.834	45		
C	1002 ± 1	18.0	39.0	0.772	42		
D	1043 ± 2	18.0	41.0	0.916	49		
Substrate material: hematite							
A - O_3	894 ± 2	18.0	39.0	0.304	16		
B	945 ± 2	36.0	41.0	0.647	35		
C	1000 ± 1	18.0	42.0	0.634	34		

[a] By use of theoretical densities of oxides given in Table II.

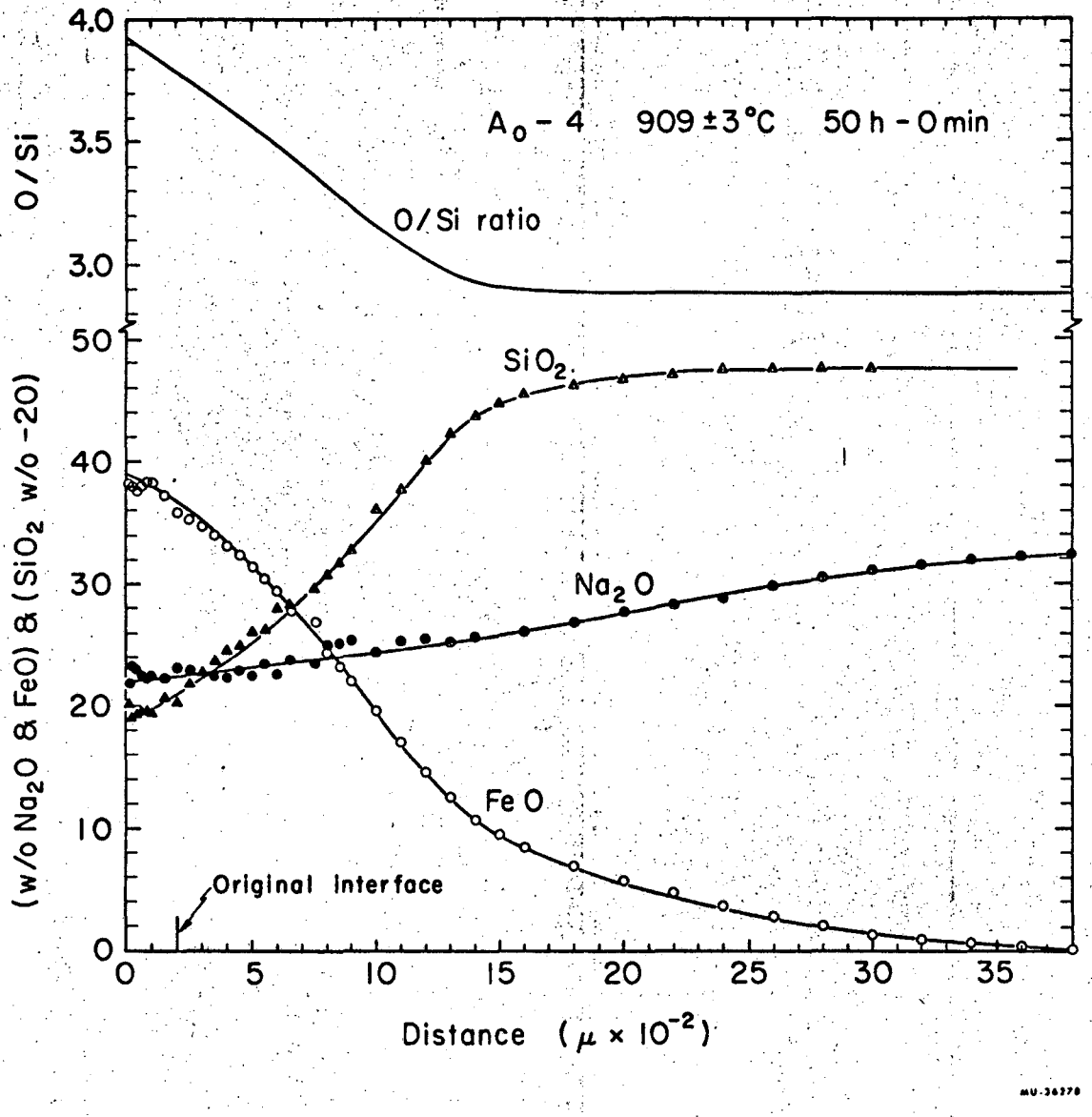

Fig. 5. Concentration profile within the glass portion of a wüstite-glass diffusion couple. The change in O/Si ratio along the diffusion path is also shown.

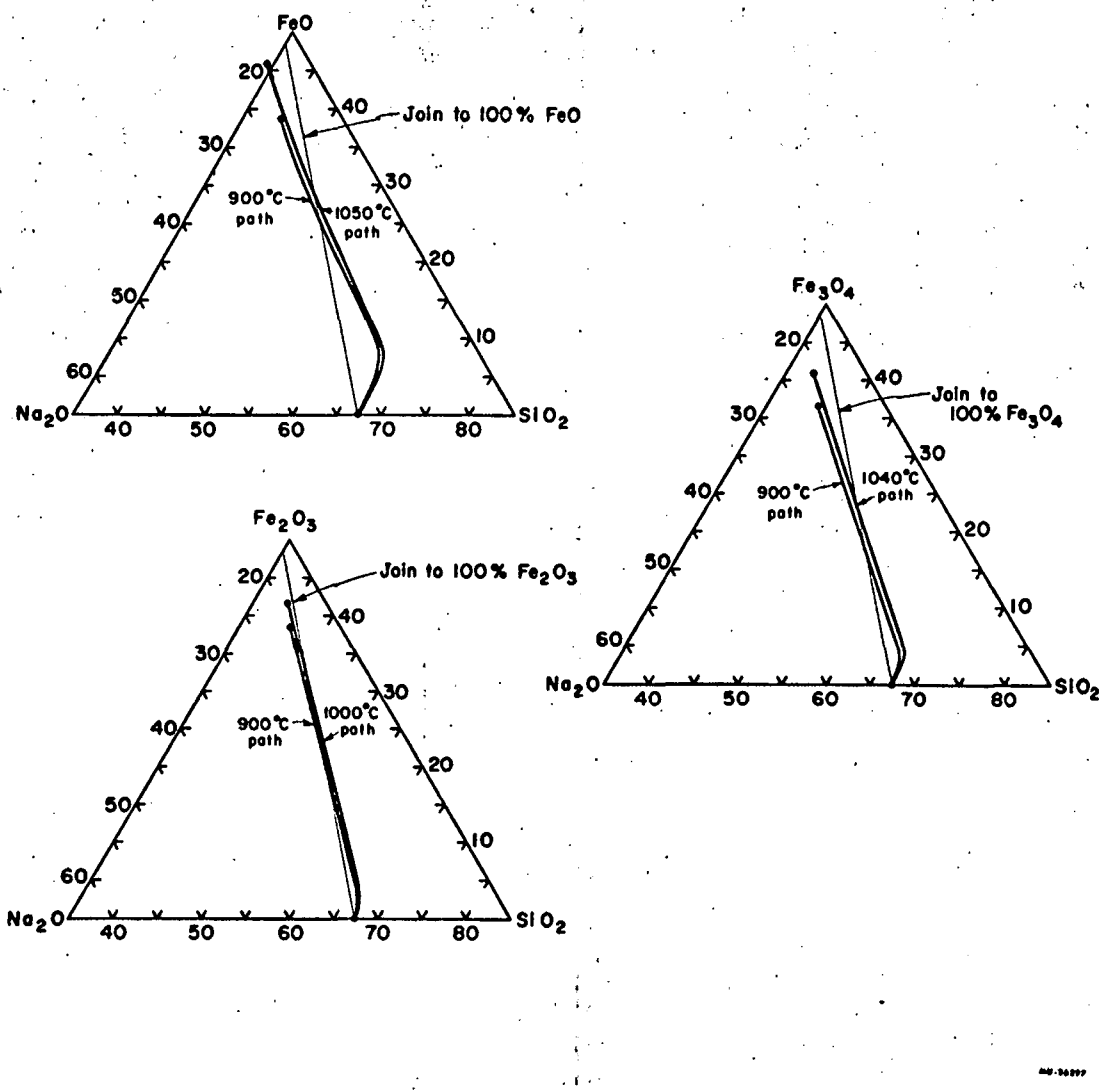

Fig. 6. Concentration paths for the diffusion couples iron oxide-sodium disilicate glass.

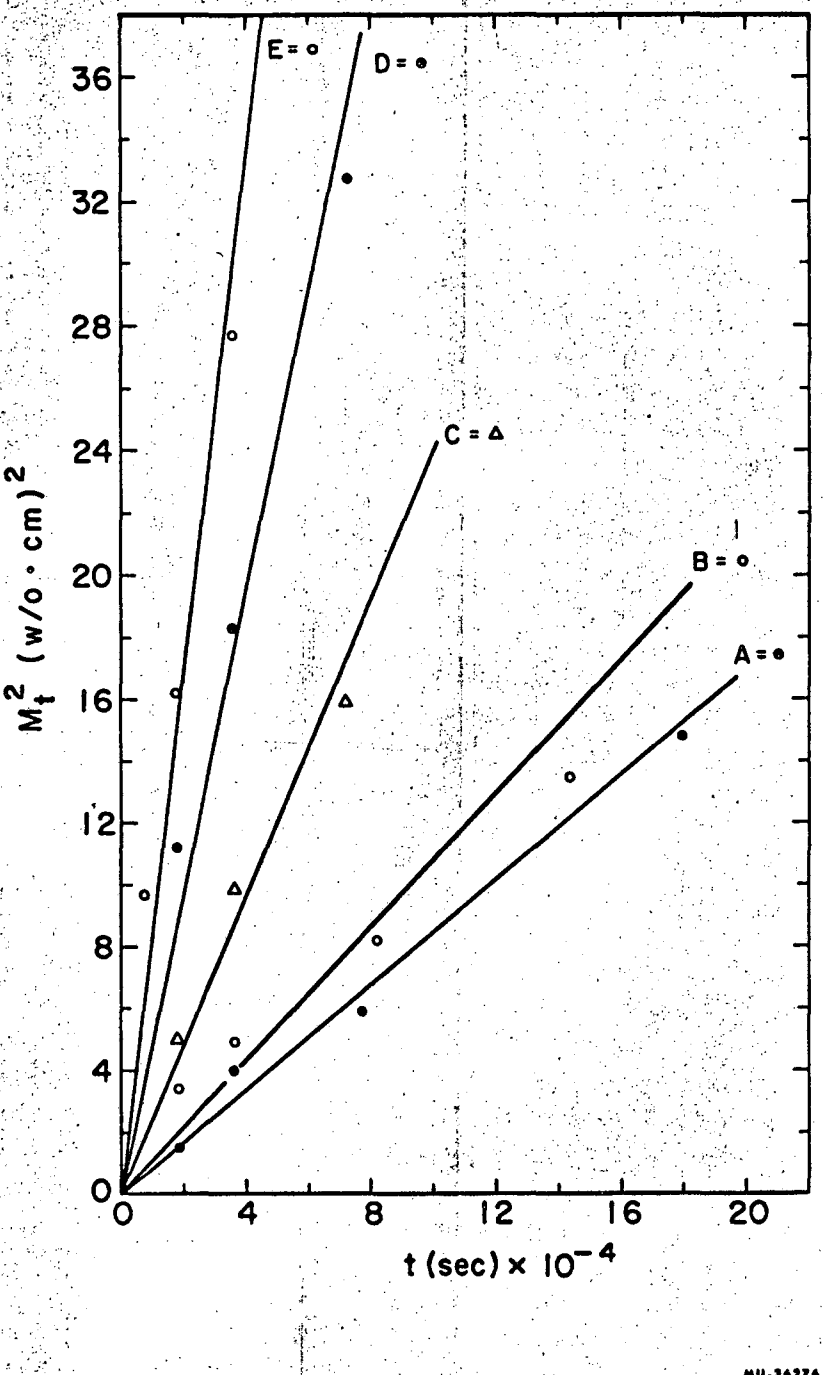

Fig. 7. Plot of the square of the total amount of wüstite dissolved, M_t^2 vs time. The approximate temperatures are A = 900°C
B = 950
C = 1000
D = 1050
E = 1100

temperature and the origin. An activation energy for the diffusion of the three oxides of iron was then determined from the Arrhenius plot of these apparent diffusivities, as shown in Fig. 8.

In order to utilize the Boltzmann approach of Eq. (5), it was necessary to determine a new $x = 0$ for each diffusion profile which satisfied the condition that ${}_0\int^{c=c_0} x\, dc = 0$. Since careful microprobe analysis at the glass-oxide interfaces detected no penetration of the components of the glass into the bulk oxide, this condition is met by determining the point x on the distance axis which gives a balance between the amount of oxide dissolved and the amount of iron oxide present as a component in the glass. The new $x = 0$ should be at the position of the original interface of the diffusion couple. In other words, the amount of iron oxide present as a component in the glass to the right of the new $x = 0$ is equal to the amount of pure iron oxide replaced by the iron-oxide-containing glass to the left of the new $x = 0$. The calculations involved here can be expressed as

$$100\, x\, \rho_{oxide} = M_t(\text{wt \% cm})\, \rho_{glass}\,, \qquad (9)$$

where ρ is the density of the respective materials.

The densities of the glasses found along the various concentration paths have not been experimentally determined, but they can be calculated from the empirically observed relationship between glass composition and density given by Morey[25] as

$$100/\rho = \sum_i W_i/d_i\,, \qquad (10)$$

where ρ is the density of the glass, d is the empirically determined density factor for each oxide component of the glass, and W is the weight percent of the oxide component in the glass. Table II gives the density and density factors of the oxide components that were used in the calculation of the glass densities.

The density of the compositions studied here varied from 2.5 g/cm^3 for sodium disilicate to approximately 3.3 g/cm^3 for the high wüstite-bearing glasses. For the calculation of the original interface by Eq. (9), the average density for the glass that was used was the density for the composition that falls on the vertical line that divides the area under the iron oxide diffusion profile into two equal portions.

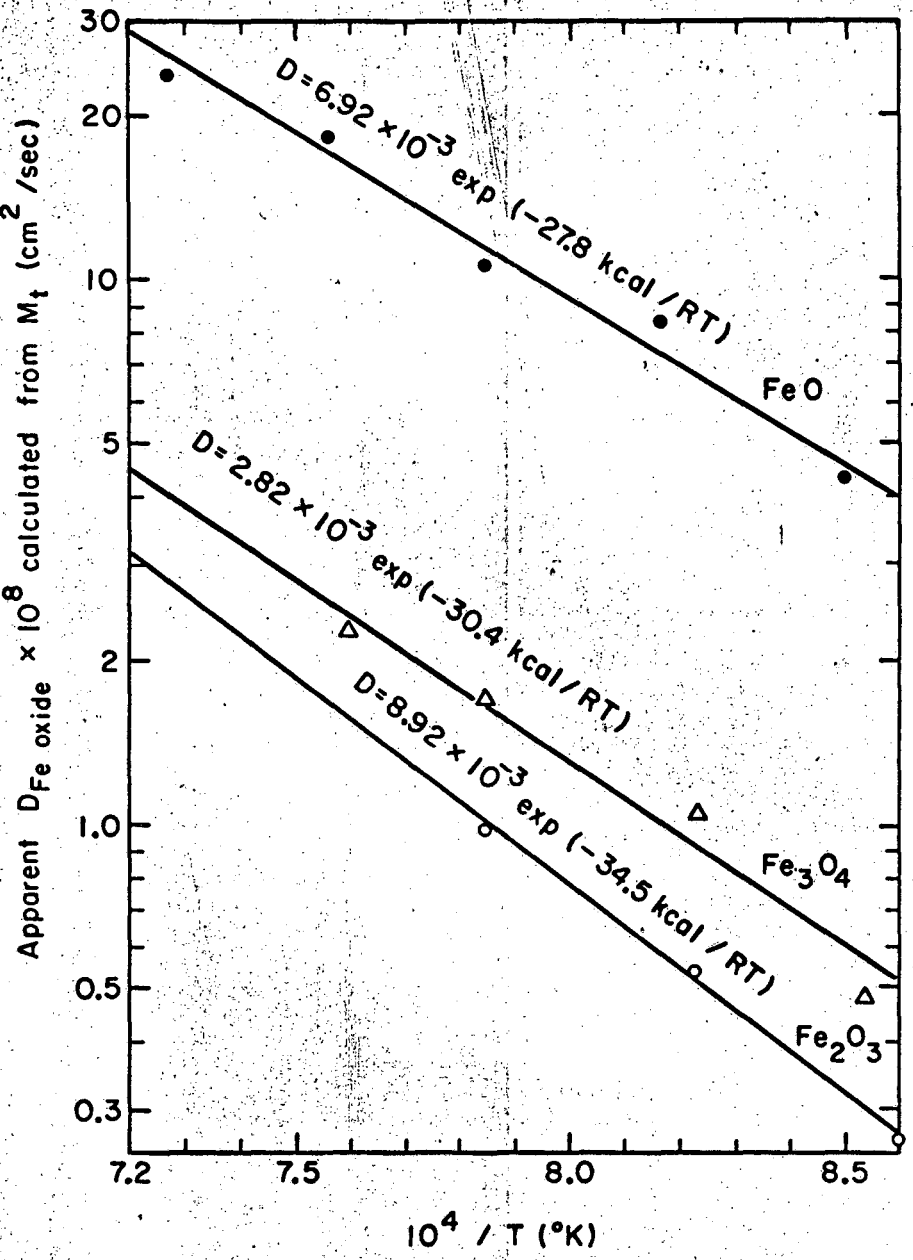

Fig. 8. Arrhenius plot of the apparent diffusivities of the oxides of iron calculated from M_t^2 vs t.

Table II. Oxide densities ρ and density factors d.

Oxide	ρ	d
SiO_2	2.2	2.3
Na_2O	2.27	3.2
FeO	5.70	4.5[a]
Fe_3O_4	5.18	4.0[a]
Fe_2O_3	5.24	3.87

a. Author's estimate.

The calculated values for the location of the original interface of the diffusion couple along with the measured values determined by using the metallic iron in the oxide and the iron ring around the oxide disks as inert markers are given in Table I. The calculated density of the wüstite also shown in Table I was determined by inserting the measured values for the original interface into Eq. (9).

The weight percent values of all the iron oxide diffusion profiles were converted to g oxide/cm^3 of glass by the appropriate density corrections, and the profiles were analyzed by the Boltzmann approach. A computer program[26] was used which determined the necessary areas and slopes from the profiles and calculated the apparent diffusion coefficients according to Eq. (5). Plots were constructed showing the variation of the apparent diffusion coefficients of the oxides of iron as a function of the mole fraction of iron oxide. Such a plot for wüstite (typical also of the shape of the magnetite curves) is shown in Fig. 9, and a plot for hematite is shown in Fig. 10. An Arrhenius plot of these D values at constant concentrations of iron oxide is given in Fig. 11.

C. Microstructures

The microstructure of the diffusion zones is worthy of comment here. The diffused region of the glass in the wüstite couples was divided into two (for the lower-temperature anneals) or three (for the higher-temperature anneals) sharply delineated color zones. Where three zones

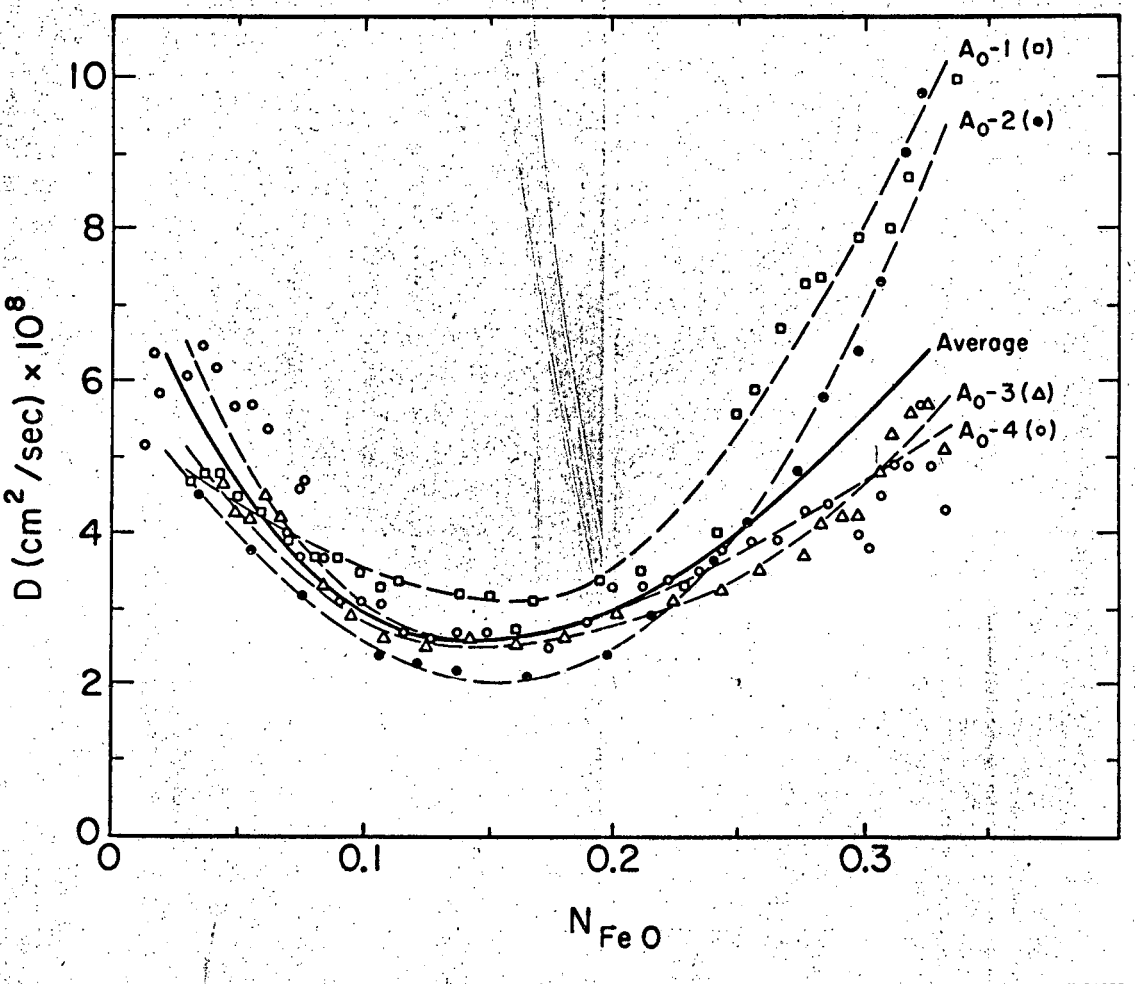

Fig. 9. Computer-determined apparent diffusivity of FeO vs mole fraction FeO. Diffusion anneals at approximately 900°C.

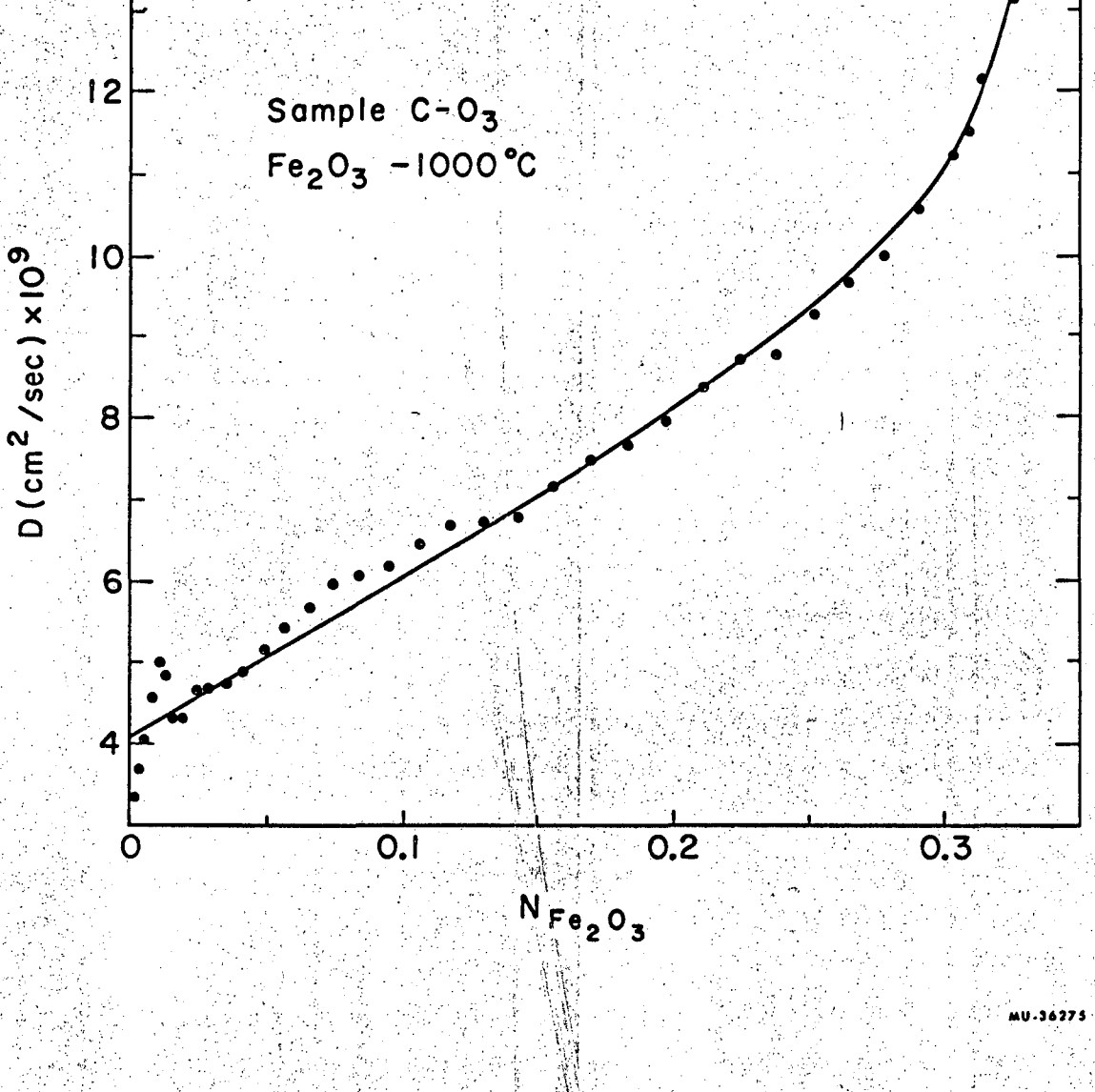

Fig. 10. Computer-determined apparent diffusivity of Fe_2O_3 vs mole fraction Fe_2O_3.

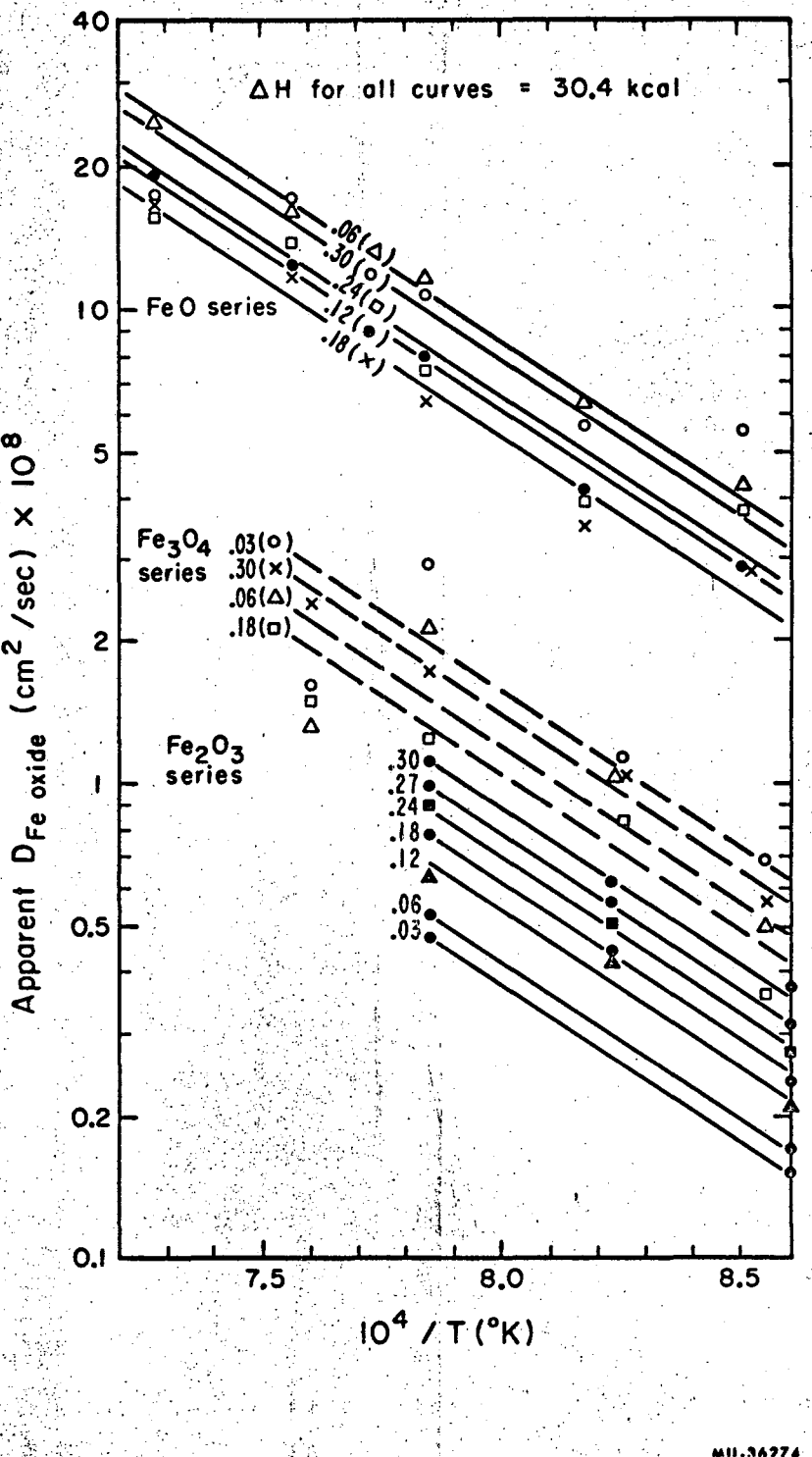

Fig. 11. Arrhenius plot of computer-determined apparent diffusivities at constant mole fractions of iron oxide.

were present the first, adjacent to the wüstite, was almost opaque to transmitted light, while the second and third were transparent and colored respectively a uniform yellowish-brown and a distinct blue grading to the colorless undiffused glass. This blue coloration is attributed to the ferrous iron in the glass. The first opaque zone mentioned here was absent from the microstructure of the lower-temperature samples. Examples of these microstructures are shown in the thin sections of Fig. 12.

An interpretation of these zones is made possible through reference to the study of the phase relationships in the system $FeO-Na_2O-SiO_2$ by Carter and Ibrahim.[27] Those glass compositions which lie on or above the FeO liquidus surface indicated by the dotted contour lines shown in Fig. 13 precipitate wüstite as the primary phase on cooling if the conditions are favorable. Whether the crystallization or devitrification actually occurs depends on such factors as cooling rate, viscosity of the liquid, and nucleation. If the above-mentioned compositions also lie within the composition triangle $F-NS_2-NFS$ shown in Fig. 13, the secondary phase, which separates on cooling, is the equimolar crystalline phase $FeO \cdot Na_2O \cdot S_1O_2$. The crystals of this phase observed by Carter and Ibrahim were feather-like, transparent, and yellowish-brown. The appearance of these crystals in the wüstite-glass couples is a result of the curved concentration path extending into the triangle $F-NS_2-NFS$ as shown in Fig. 13. It is emphasized that this phase separation is a cooling phenomenon, and is not the result of reactions occurring at the test temperature. As the liquidus composition becomes richer in FeO (higher-temperature anneals) it becomes more difficult to prevent devitrification and the FeO primary phase separates easily on cooling; for the lower-temperature diffusion anneals the primary phase is not observed and the devitrification apparently occurs at lower temperatures with the separation of the secondary phase.

Extensive phase separation, as in the high-temperature anneals, complicates electron microprobe analysis of the profiles because of the presence of large crystals, which were not present at the anneal temperature. As a result microprobe analysis of the zone of crystallization for the 1100°C anneals showed an almost constant equimolar composition of the three oxide components over the length of this zone.

Fig. 12. Microstructures of the interfacial region of the diffusion zones of samples B_0-4 and E_0-3.

The interfacial region is divided into 3 sections: (A) glass portion of the diffusion zone, (B) devitrified portion of the diffusion zone, and (C) undissolved wüstite.

(a) Sample E_0-3, showing extensive primary separation of wüstite adjacent to substrate and secondary-phase separation extending further into the diffusion zone.

(b) Detail of photomicrograph (a).

(c) Sample B_0-4, showing occurrence of feather-like crystals which are believed to be $FeO \cdot Na_2O \cdot SiO_2$.

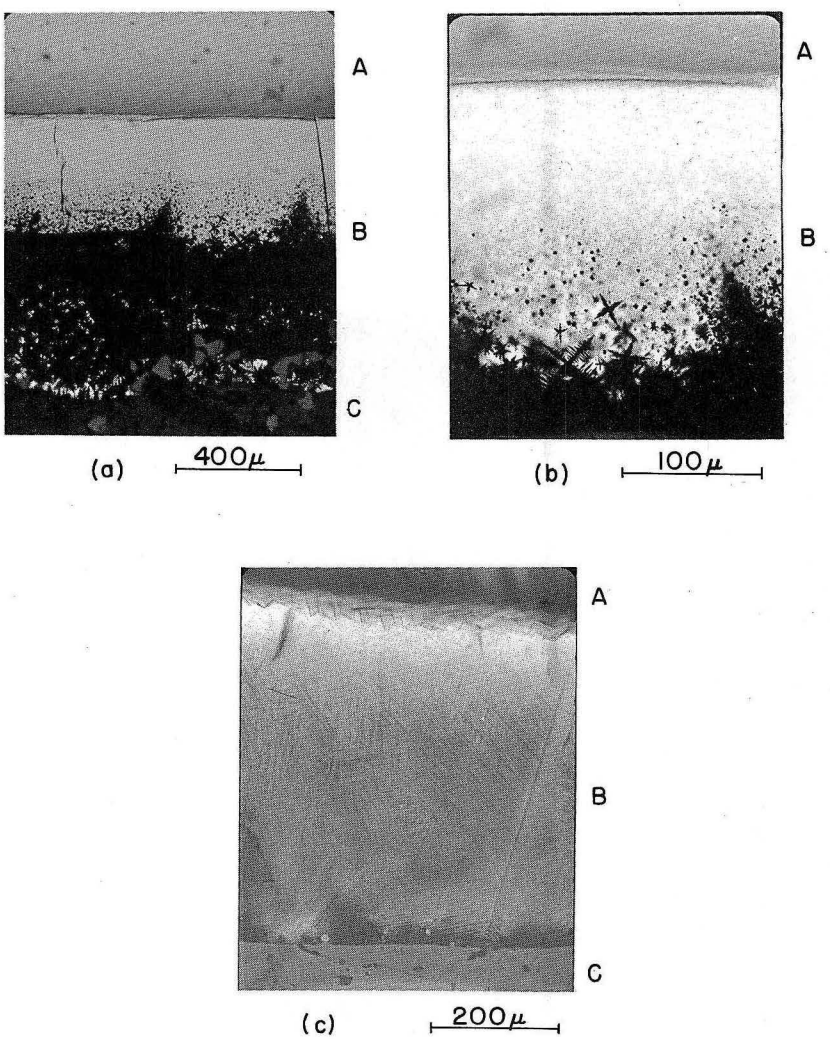

ZN-5087

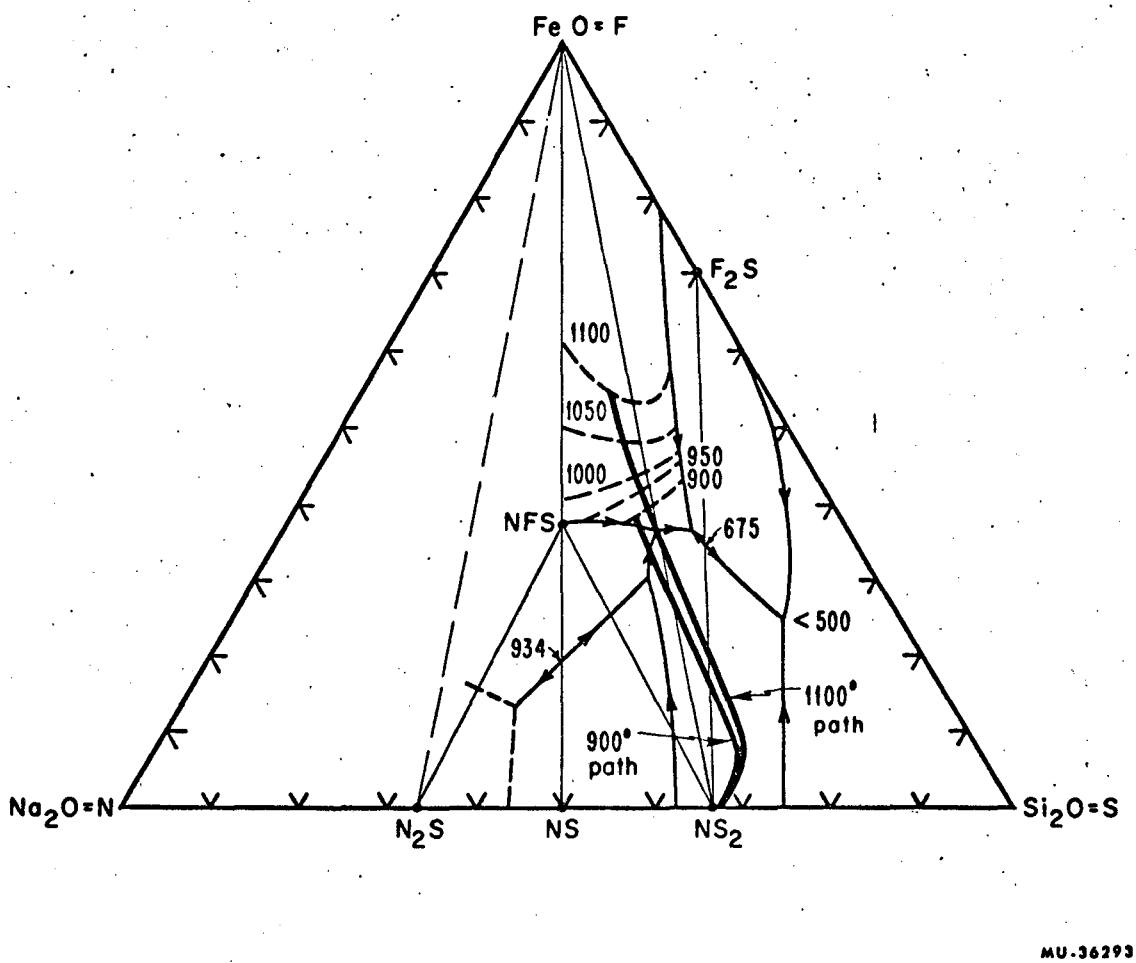

Fig. 13. Phase diagram (wt %) of $FeO-Na_2O-SiO_2$ system showing composition paths for diffusion couple $FeO-Na_2O \cdot 2SiO_2$.

This is, in part, a result of having consciously avoided including the visible dendrites of wüstite in the analysis. In these cases the at-temperature profiles were constructed by extrapolation to the appropriate liquidus compositions shown on Fig. 13.

The diffusion zone in the hematite-glass couples was observed to be reddish-brown grading in intensity to the colorless undiffused glass. The color generally associated with ferric ions in glass is yellow.[28] It is assumed that the coloration observed here is due to finely dispersed crystals of Fe_2O_3 which have precipitated during the cooling of the sample. The finely dispersed nature of this phase separation and the small size of the crystals relative to the beam diameter does not complicate the microprobe analysis of these couples. This is indicated by the fact that the concentration distributions so determined are smooth and the liquidus compositions compare favorably to compositions expected on the basis of the known phase diagram.[29]

The diffusion zones of the magnetite-glass couples were similar in coloration to those of the hematite series with the exception that the leading edge of the zone in the glass was greenish in color. The phase relations in this system have not been previously studied, and no correlations can be made from the literature.

V. DISCUSSION OF RESULTS

A. Diffusion-Controlled Dissolution

Evidence of the diffusion-controlled nature of the dissolution of wüstite is found in several considerations of the experimental data. The straight-line plots of Fig. 7 and the fact that the square of the penetration distance for a given concentration was found to be a linear function of the diffusion time confirm the applicability of diffusion mathematics to this process, but they do not conclusively establish that diffusion in the liquid is rate-controlling. This latter point is clarified by the fact that the glass composition at the interface remains constant with time and is a function only of temperature. If the slow step were the rate of transfer of material across the interface (i.e., if diffusion in the liquid were faster than the dissolution rate) the observed concentration of FeO in the glass at the interface would increase with time, and approach but never reach the liquidus composition. The same concentration paths shown in Fig. 13 would apply, except that their extension to the liquidus would not be complete.

Since there is insufficient experimental evidence here, the assumption was made that the dissolution of both magnetite and hematite is similarly controlled by diffusion in the liquid phase. If this is the case, the concentration distributions should be unaffected by the choice of either a single crystal or a polycrystalline substrate. This assumption is in part justified by the fact that random orientations of single-crystal stock of magnetite and hematite were employed in these studies with no anomalous results attributable to crystal orientation.

B. Calculations Based On Equations For Binary Diffusion

The plots of Figs. 7 and 8 based on the total amount of oxide dissolved give information regarding only the average apparent diffusivity, or the interdiffusivity, between the oxide and the glass, and the average activation energy for the process, and give no direct evidence of the diffusivities of the individual species. This approach, however, can be used as a first approximation and in the absence of a suitable means of determining the concentration distribution within the glass. Tashiro[11]

in 1949 studied the dissolution of iron oxide by an enamel by measuring the rate at which the thickness of an oxide layer diminished with time. His calculations were based on the differentiation of Eq. (3) with respect to time to give

$$dM_t/dt = C_s(D/t\pi)^{1/2} . \qquad (11)$$

Assuming a Gaussian solution for a binary system in which the surface concentration remains constant, one finds for the penetration distance, x,

$$(x)_{c=c_1} = K(Dt)^{1/2} . \qquad (12)$$

Substitution of Eq. (12) into (11) yields

$$\frac{dM_t}{dt} = D \frac{K}{\pi^{1/2}} \frac{C_s}{(x)_{c=c_1}} , \qquad (13)$$

where $K/\pi^{1/2}$ is a constant slightly greater than unity. Equation (13) can be compared with the equation used by Tashiro,

$$\frac{dM}{dt} = S \frac{d\ell}{dt} = D \frac{C_s}{(x)_{c=c_1}} , \qquad (14)$$

in which S is the density of ferrous oxide and ℓ is the diminished thickness of the oxide layer. Tashiro calculated a value for $D_{FeO} = 6.6 \times 10^{-8}$ at 885°C where the saturation value of the FeO in the enamel, C_s, was known. This point is shown for comparison on Fig. 14. His calculation of an activation energy of 53 kcal for diffusion was based on the relationship

$$S \frac{d\ell}{dt} = (\text{const}) \frac{C_s}{(x)_{c=c_1}} \exp\left(-\frac{\Delta H}{RT}\right) , \qquad (15)$$

and the assumption that since both C_s and $(x)_{c=c_1}$ increase exponentially with temperature, the ratio $C_s/(x)_{c=c_1}$ is a constant independent of temperature. The higher activation energy observed by Tashiro for this process could easily be explained if C_s increased more rapidly with temperature than $(x)_{c=c_1}$.

C. Effect of Porosity on the Diffusion Profiles

Some additional observations can be made at this point regarding the diffusion profiles and the microstructure of the wüstite-glass diffusion couples. Table I shows that the measured reduction in thickness of

the wüstite substrate is generally greater than the calculated reduction. The calculated density of the oxide, based on the measurement of the actual reduction in thickness, indicates a porosity of about 20% in the substrate. This agrees favorably with the porosity observed under the microscope if one also considers the particles of excess iron as contributing to the pore volume. This is reasonable, since the glass also sees this iron as inert particles or voids. The thickness of the oxide is, therefore, diminished more rapidly in regions of higher porosity or excess iron content or both; however, the concentration distribution, which is controlled by diffusion in the liquid phase, is unaffected by these fluctuations in penetration rate. In addition, large oblate spheroidal pores are observed at the interface. It was observed that these pores also have no effect on the concentration distributions, which extend smoothly from one side of the pore to the other just as if there were glass present instead of a void. This phenomenon is attributed to surface diffusion rates that are much faster than bulk diffusion rates, and therefore able to maintain the necessary supply of material across the void. The pores themselves are probably the accumulation of the bypassed true porosity in the oxide, and their shape is probably due to the increase in viscosity away from the interface.

D. Ternary Diffusion

Some questions may be raised regarding the applicability of ternary diffusion kinetics to these systems, which have in actuality four and in some cases five diffusing species. This problem can be resolved by considering the following possibilities.

(a) If oxygen is the fastest diffusing species in a system containing three oxide components, the elimination of any concentration gradients is controlled solely by the diffusion of cations. Oxygen can distribute itself in whatever may be necessary in order to maintain electroneutrality. This has been found to be the case in calcium-aluminum-silicate slags above 1400°C.[14,30,31]

(b) If oxygen diffuses more slowly than the cation of the dissolving or solute oxide, it can be shown that the liquidus composition will be maintained even though the solute cation may be able to exchange with other

cations in the glass without requiring a coupled motion of the oxygen. In this case the dissolution is still controlled by the diffusion of the cation species, and the oxygen can be accounted for by associating it with the cations in such a fashion as to maintain electroneutrality (i. e., expressing the concentrations in terms of the oxide components).

(c) If considerations (a) and (b) hold, then the intermediate case, in which the oxygen diffuses faster than the solute cation but is not itself the fastest diffusing species in the system, should also hold.

Case (c) above appears to apply to the systems under study. Data for the self-diffusion of oxygen in two glasses[30,32] are shown in Fig. 14. The self-diffusion coefficients of oxygen in fused silica are known[33] but are, however, too low to be shown on the figure. It appears that the mobility of the oxygen increases with an increase in the alkali content of the glass. On the basis of the data shown on Fig. 14 it is then not unreasonable to assume that the mobility of the oxygen in the systems under study would exceed the mobility of the solute cation. One might expect that the mobility of the silicon in these systems would also be higher than the values shown on Fig. 14, but not necessarily so high as that for the solute cation.

The hematite-glass couples represent the only true ternary system encountered here. The wüstite and magnetite couples are complicated respectively by the presence of approximately 8 wt % and 45 wt % ferric ions. No attempt has been made here to separately determine the concentration distributions of the two valences of iron in the wüstite and magnetite couples. It is believed, however, on the basis of the color distribution in the wüstite couples and the relative diffusivities of the ferric and ferrous ions indicated by Figs. 8 and 11, that the diffusion of the ferric ions in the wüstite couples does not greatly influence the concentration distribution of the iron. To a first approximation, then, these couples may be treated as representing a true ternary system. Greater errors are certainly involved in applying this approximation to the magnetite couples, but the magnitude and nature of this error are not known.

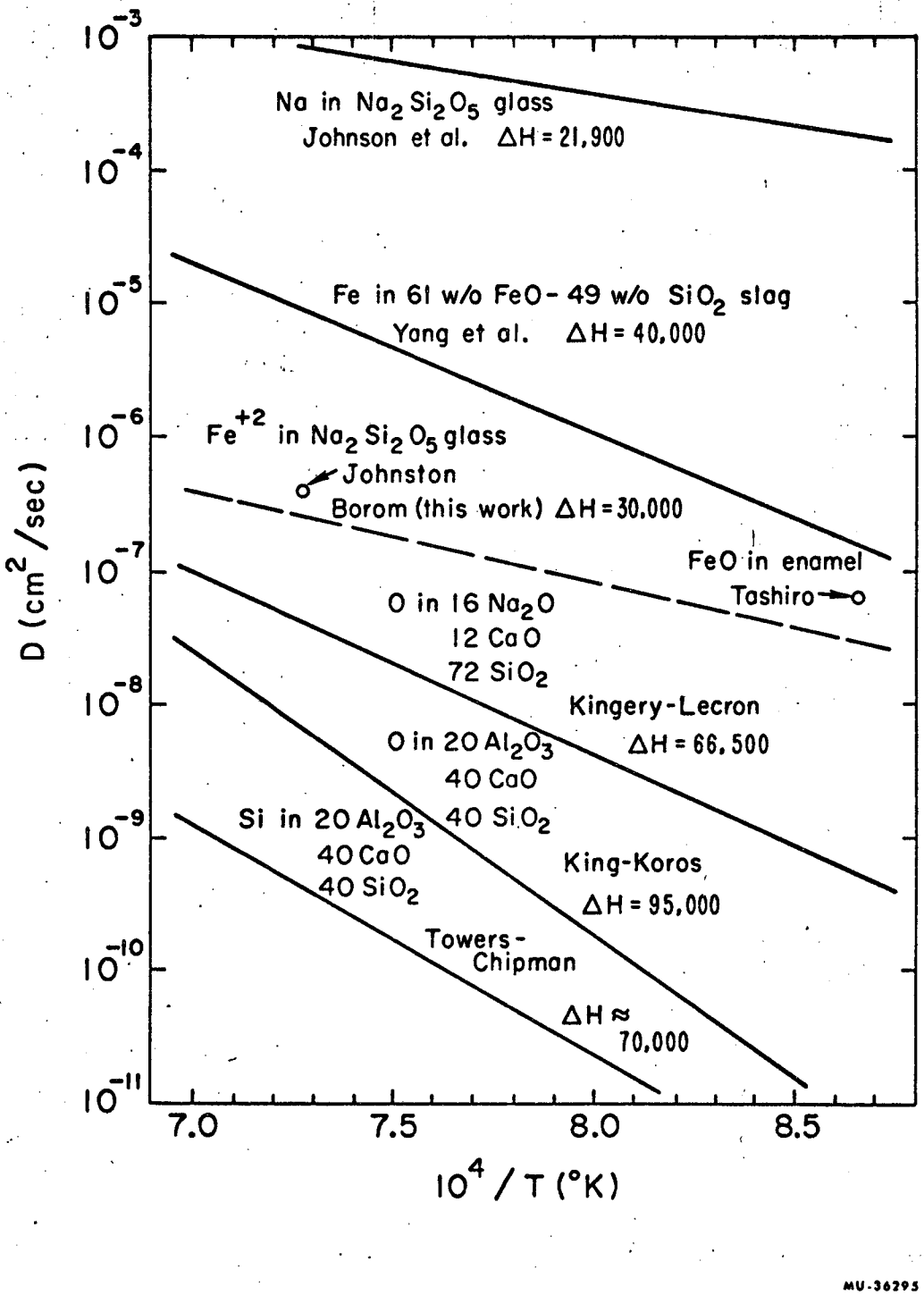

Fig. 14. Arrhenius plot of available data from literature.

E. Calculations Based on Equations for Ternary Diffusion

As pointed out earlier, the apparent diffusivities calculated here by the Boltzmann method may be interpreted in terms of the self-diffusion coefficients of the individual cations by means of Eq. (6). The equation may be simplified by comparing the self-diffusion data shown in Fig. 14 for sodium[34] and silicon. Even considering that the diffusivities of silicon in the glasses used in this study are probably higher than the values shown in Fig. 14, it remains apparent that the diffusivities of sodium are orders or magnitude greater than those of either iron or silicon. This is verified experimentally for silicon by measuring the concentration gradients of Na_2O and SiO_2 at $x = 0$ (see Fig. 5) and substituting into the equation derived by Oishi et al.,[14]

$$\frac{D_{Na_2O}}{D_{SiO_2}} = \frac{\text{wt \% } Na_2O}{\text{wt \% } SiO_2} \frac{\text{grad } SiO_2}{\text{grad } Na_2O} . \tag{16}$$

Consider now only the bracketed term of Eq. (6),

$$D_{app} = \frac{N_1 + N_2}{N_1 D_2 + N_2 D_1} (N_1 D_2 D_3 + N_2 D_3 D_1 + N_3 D_1 D_2) , \tag{17}$$

which can be rewritten as

$$D_{app} = (1 - N_3)\, D_3 + \frac{(1 - N_3)\, N_3 D_1 D_2}{N_1 D_2 + N_2 D_1} . \tag{18}$$

Since D_{Na} is always an order of magnitude greater than D_{Si}, Eq. (18) can be simplified to read

$$D_{app} = (1 - N_{Fe})\, D_{Fe} + \frac{(1 - N_{Fe})\, N_{Fe}}{N_{Si}} D_{Si} , \tag{19}$$

where the subscripts refer to the oxides. Equation (19) applies strictly only at the interface; however, the data indicate that it can be used for a qualitative discussion of the apparent diffusivity of iron oxide in the bulk glass.

Equation (19) can be compared with Darken's equation for binary diffusion,

$$D_{app} = D_A N_B + D_B N_A . \tag{20}$$

In ideal binary diffusion D_A and D_B are the self-diffusion coefficients of components A and B in the pure materials, and they do not vary with composition. If, however, the system deviates from ideality Eq. (20) must be either multiplied by the appropriate concentration-dependent

correction factor or expressed in terms of the self-diffusion coefficients characteristic of each composition.

Under ideal conditions D_{app} of Eq. (19) is the sum of two essentially linear functions, and is expressed graphically in Fig. 15. It can be seen from Fig. 15 that if the glasses under study are ideal solutions a plot of D_{app} vs mole fraction iron oxide should yield a straight line, the slope of which would depend on the relative diffusivities of iron and silicon. If $D_{Fe} \gg D_{Si}$ the slope would be negative and equal to D_{Fe}. If $D_{Si} = 2/3\ D_{Fe}$ the plot would yield a horizontal line, and for any value of D_{Si} greater than this the slope would be positive. If the glasses deviate from ideality these plots are no longer linear, but have some curvature depending on the degree of deviation.

Consider now the variation of the apparent diffusivity of FeO with concentration, as shown in Fig. 9. The curve begins from the origin with a considerable negative slope, which implies that $D_{Fe} > D_{Si}$ and that the curve is governed by the function $Y_{Fe} = (1 - N_{Fe})\, D_{Fe}$. The change of the slope from negative to positive with an increasing FeO content is the result, as discussed above, of a deviation from ideality that brings about an increase in the diffusivity of the iron. This change in diffusivity over the range of iron composition appears to be by no more than a factor of two or three. The diffusivities of the other components should also be expected to increase with increasing iron content, but no measure of that can be gained from these curves. This increase in the self-diffusion coefficients is discussed in relation to a change in the glass structure in a later section.

The curves of apparent diffusivity vs mole fraction Fe_3O_4 are similar to those for FeO with the exception that the initial negative slope is less. This indicates that the diffusivities of the iron and the silicon are not quite so dissimilar as in the FeO, and a contribution is being made by the function containing the diffusivity of the silicon.

The shape of the curve for Fe_2O_3 shown in Fig. 10 is, however, quite different. The slope begins positive and becomes increasingly greater. From the above considerations we know that $D_{Si} > 2/3\ D_{Fe}$. The straight-line portion of the curve holds up to about $N = 0.18$. The intercept of this portion with the ordinate gives $D_{Fe} = 4 \times 10^{-9}$ cm^2/sec. Extrapolation of this portion of the curve to $N = 1.0$ permits the

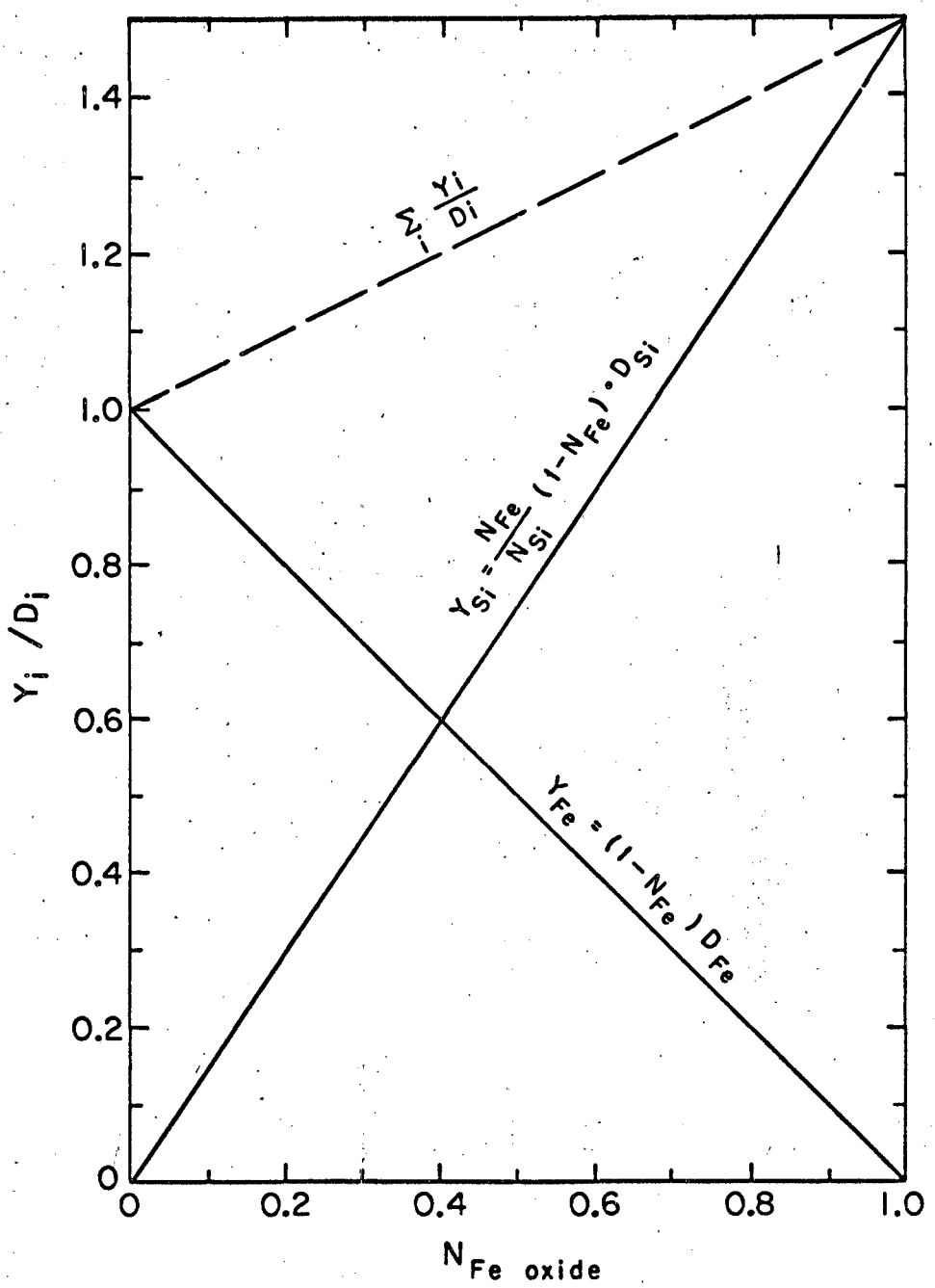

Fig. 15. Plot of the functions that comprise the simplified apparent diffusion coefficient for the oxides of iron vs mole fraction iron oxide. The subscripts refer to the oxides.

calculation of a value for $D_{Si} = 1.6 \times 10^{-8}$. The diffusion coefficient of Si^{+4} then appears to be about four times that for Fe^{+3} at 1000°C. The type of concentration dependence observed for the other oxides of iron is also in evidence here.

F. Concentration Paths

Some immediate qualitative information can be gained from an examination of the concentration paths shown in Fig. 6. Oishi[15] has shown mathematically that a linear concentration path for the general case in ternary diffusion is realized only when $D_1 = D_2 = D_3$, but that there are special cases in which only two diffusivities need be equal to produce a linear concentration path. A special case is given by a diffusion couple whose end members lie along the same straight line drawn through a corner of the triaxial composition diagram; these conditions are found in this dissolution study. Oishi has shown that under these conditions a linear concentration path will result if the self-diffusion coefficients of the solvent species are equal (i.e., $D_1 = D_2$), regardless of the value, D_3, of the solute species. It can be shown, however, by the same mathematical argument for this case that a linear path also results if either $D_3 = D_1$ or $D_3 = D_2$. It follows from these observations that the greatest curvature is to be expected when the D values for the three components are most dissimilar. For the actual case at hand, since D_{Na} always has the highest value, the greatest curvature is found when either $D_{Na} > D_{Fe} > D_{Si}$ or $D_{Na} > D_{Si} > D_{Fe}$. It is reasonable to expect that the former sequence applies, since the higher charge on the silicon should result in a lower diffusivity. From Fig. 6 one may surmise from the curvatures that $D_{Na_2O} > D_{FeO} > D_{SiO_2}$, $D_{Na_2O} \gg D_{Fe_3O_4} > D_{SiO_2}$, and $D_{Na_2O} \gg D_{Fe_2O_3} \approx D_{SiO_2}$.

The general curvature assumed by the concentration paths of Fig. 6 is due to the fact that $D_{Na} > D_{Si}$ and does not depend on the value of D_{Fe}. If it were that $D_{Si} > D_{Na}$, the concentration paths would be mirrored across the join to 100% iron oxide. It is interesting to note that this relationship between D_{Na} and D_{Si} produces a range of compositions in the low iron region in which the silica content, and consequently the O/Si ratio, is essentially constant. This region is most

extensive for the FeO series (see Figs. 5 and 6) and least extensive for the Fe_2O_3 series. It is in this region that the self-diffusion coefficient of iron is least affected by composition changes in the glass. This is attributed to the fact that the basic silica framework of the glass is not changing, and interdiffusion is taking place primarily between iron and sodium.

G. Activation Energies

An Arrhenius plot of the apparent diffusivities at constant mole fractions of the three oxides is given in Fig. 11. The best straight-line fit is obtained for the FeO data in which each point represents the average of three or four determinations. Fair agreement is obtained for the Fe_2O_3 data (true ternary), and the most scatter is found for the Fe_3O_4. As has been shown above, the diffusion coefficients for the iron cations are not directly given by this plot; however, a close approximation to the true self-diffusion coefficient of the iron cations is given by the lines representing the lowest mole fraction of iron oxide. It is interesting to note that, if we consider the lines for $N = 0.06$, the values for magnetite are approximately intermediate between those of wüstite and hematite. It is also interesting to note that the slope of all the lines is the same, and give an activation energy for the process of 30.4 kcal.

A comparison of the two methods of computing activation energies for diffusion (see Figs. 8 and 11) shows that they yield values for the activation energy that are consistent within ± 10%. The plots of Fig. 8 are almost coincident with the plots in Fig. 11 for $N = 0.30$. The method of Fig. 8 then gives an apparent diffusivity that is characteristic of the high-concentration end of the iron profile. Because of the nature of the distribution of the apparent diffusivities, the magnetite and wüstite plots are also almost coincident with the lines for $N = 0.06$.

The Arrhenius plot for $N_{FeO} = 0.06$ is shown on Fig. 14 for comparison with the available data from the literature. The values for Fe^{+2} and FeO reported by Johnston and Tashiro respectively compare favorably with the data of this study. The data of Yang et al. for the self-diffusion of Fe^{+2} extrapolated from a narrow range of determinations

at higher temperatures cannot be directly compared because of the composition differences in the glasses; however, it is in the direction to be expected on the basis of the work of Le Clerc.[35] Le Clerc found that if a potassium silicate glass were mixed with a sodium silicate glass the self-diffusion coefficients of each of the alkali or network-modifying cations was depressed, and the smaller cation was more strongly affected by this mixing. This was the result of self-diffusion of the two types of ions taking place through equivalent positions in the glass structure. It is reasonable to expect, then, that the activation energy for the diffusion of iron ions in a sodium silicate glass should lie, as observed here, between the values reported by Johnson et al. and by Yang et al., shown on Fig. 14.

H. Concentration Dependence

Some insight may be gained into the mechanisms of the diffusion process by analyzing the data in the light of the present concepts of glass structure. The basic building block of silicate glasses is a tetrahedral unit composed of a silicon atom surrounded by four oxygen atoms. These tetrahedral units link together to form chains or the glass network by sharing corners. In fused SiO_2 each oxygen is shared by two silicon atoms; these are referred to as bridging oxygens. The silicon atoms are directionally and covalently bonded to the oxygen atoms. If another oxide, such as soda, whose cation is more ionic in nature, is added to the glass a new type of position is formed in the glass structure. The oxygens surrounding this new cation are shared by the new cation and silicon rather than by two silicons; these oxygens are referred to as nonbridging. The O/Si ratio can be taken as a measure of the number of these nonbridging oxygens that exist in the glass structure. In fused silica, in which there are no nonbridging oxygens, the O/Si ratio is 2. If all the oxygens of the tetrahedral unit were nonbridging the ratio would be four or greater.

Accordingly, as one adds an oxide of a more ionic nature to a molten silicate glass, the structure within the glass is altered through the formation of more nonbridging oxygens and consequently more glass-modifier positions. One might suspect, then, that the self-diffusion coefficients of the constituents of the glass would be affected by this change in

structure. Johnson et al. have shown that the self-diffusion coefficient of sodium in sodium silicate glasses increases rather strongly with an increase in the sodium content (i.e., an increase in the O/Si ratio), even though the activation energy for diffusion remains unchanged. This is analogous to the cases here for each of the oxides of iron in which an entire range of compositions with a change in O/Si ratio is found within each concentration distribution (see Fig. 5). Not only is the activation energy independent of composition for the cases studied here, but it is also independent of the oxide of iron used. The implication is that the activation energy for the diffusion of iron is predominantly characteristic of the exchange of the cations in the glass-modifying positions, and is independent of the number of these positions. The diffusivity itself, however, can be strongly affected by the number of these positions, since the preexponential term of Eq. (8) contains the probability of having an appropriate adjacent site for diffusion. The lower diffusivity of the ferric ion is probably due to the higher charge it bears, requiring an exchange with a greater number of lower-valence cations.

VI. CONCLUSIONS

The following conclusions have been drawn regarding the systems studied in this report:

1. The dissolution of each of the oxides of iron by sodium disilicate glass is controlled by diffusion in the molten glass.

2. An approximate measure of the diffusion kinetics pertaining to these systems can be gained by employing the mathematics for binary systems. This can be accomplished without any knowledge of the concentration distributions in the glass; one need only know the concentration, C_s, of the iron oxide which saturates the glass and the total amount of iron oxide, M_t, introduced into the glass in a given time.

3. A more exact analysis of the diffusion kinetics can be gained from the use of the mathematics for ternary diffusion. The treatment is greatly simplified here, since D_{Na} is much greater than either D_{Fe} or D_{Si}.

4. The self-diffusion coefficients of iron and silicon can be estimated from the data, and they are shown to increase with increasing concentrations of iron (i.e., increasing O/Si ratio). This increase in the self-diffusion coefficients is related to changes occurring in the glass structure, as indicated by the increase in the O/Si ratio.

5. The relative diffusivities of the cation species are shown to be

$$D_{Na^+} \gg D_{Fe+2} > D_{Si+4} \geq D_{Fe+3} .$$

Over the range of temperature 900° to 1100°C the self-diffusion coefficients of ferrous iron are found to be an order of magnitude greater than those for ferric iron.

6. The activation energy for the diffusion of each of the oxides of iron as calculated by ternary diffusion mathematics was found to be the same and equal to 30.4 kcal. The activation energy was also found by these calculations to be independent of the glass composition.

7. The activation energies for diffusion calculated by binary diffusion mathematics were 27.8 kcal for FeO, 30.4 kcal for Fe_3O_4, and 34.5 kcal for Fe_2O_3, but it is not certain whether any significance can be attached to this variation.

ACKNOWLEDGMENTS

I extend grateful appreciation to Joseph A. Pask for his guidance and encouragement of this research, to Yas Oishi and John E. Dorn for many helpful discussions, to William L. Jolly and John E. Dorn for their criticisms and comments regarding this paper, to Bernard Evans for instruction and help in the use of the electron microprobe, to Roy Wright of the Philadelphia Quartz Company for the chemical analysis of the standard glasses, and to the staff and personnel of the Inorganic Materials Research Division of the Lawrence Radiation Laboratory for their support.

I especially acknowledge the patience and encouragement of my wife, Maxine, which have contributed greatly to the success of these past four years.

This work was conducted under the auspices of the U. S. Atomic Energy Commission.

REFERENCES

1. W. Eitel, Silicate Science, Volume II, Glasses, Enamels, Slags, (Academic Press, New York and London, 1965), pp. 538-547.
2. J. A. Pask and R. M. Fulrath, Fundamentals of Glass-to-Metal Bonding: VIII, Nature of Wetting and Adherence, J. Am. Ceram. Soc. 45 [12], 592 (1962); J. A. Pask, Glass-Metal "Interfaces" and Bonding, in Modern Aspects of the Vitreous State, Vol. 3, J. D. Mackenzie, Ed. (Butterworths, Washington, 1964); pp. 1-28.
3. B. W. King, H. P. Tripp, and W. H. Duckworth, Nature of Adherence of Porcelain Enamels to Metals, J. Am. Ceram. Soc. 42 [11], 504 (1959).
4. J. A. Pask and M. P. Borom, Physical Chemistry of Glass-Metal Interfaces, in Proceedings of the 7th International Congress on Glass, Brussels, July, 1965 (to be published) (Lawrence Radiation Laboratory Report UCRL-11816 Rev., May 1965).
5. M. P. Borom and J. A. Pask, The Role of Adherence Oxides in the Development of Chemical Bonding at Glass-Metal Interfaces, J. Am. Ceram. Soc. (to be published).
6. M. P. Borom, J. Longwell, and J. A. Pask, Reactions between Iron and Sodium Disilicate Glass Containing Cobalt Oxide, unpublished data.
7. M. P. Borom, Diffusion of Iron into Sodium Disilicate Glass (M.S. Thesis) Lawrence Radiation Laboratory Report UCRL-11116, Nov. 1963, plus additional unpublished data, University of California, Berkeley.
8. E. L. Williams, Diffusion Studies in Glass. I, Glass Industry 43 [3], 113-17 (1962); II, ibid. [4], 186-91; III, ibid. [5], 257-61; IV, ibid. [7] 394-95, 402; Appendix, ibid [8], 437-40 (1962).
9. L. Yang, C. Chien, and G. Derge, Self-Diffusion of Iron in Iron Silicate Melt, J. Chem. Phys. 30, 1627 (1959).
10. W. D. Johnston, Oxidation-Reduction Equilibria in Iron-Containing Glass, J. Am. Ceram. Soc. 47 [4], 198-201 (1964).
11. Megumi Tashiro, Mechanism of Adherence of Enamel to Steel Surface, III, J. Japan Ceram. Assoc. 57, 124-25 (1949); IV, ibid. 149-50; V, ibid. 58, 51-54 (1950); cf. Ceram. Abstracts, 1951, 3-4, 23, 61.

12. A. R. Cooper, Jr., and W. D. Kingery, Dissolution in Ceramic Systems: I, Molecular Diffusion, Natural Convection, and Forced Convection Studies of Sapphire Dissolution in Calcium Aluminum Silicate, J. Am. Ceram. Soc. 47 [1], 37-43 (1964).
13. B. N. Samaddar, W. D. Kingery, and A. R. Cooper, Jr., Dissolution in Ceramic Systems: II, Dissolution of Alumina, Mullite, Anorthite, and Silica in a Calcium-Aluminum-Silicate Slag, J. Am. Ceram. Soc. 47 [5], 249-50 (1964).
14. Y. Oishi, A. R. Cooper, Jr., and W. D. Kingery, Dissolution in Ceramic Systems: III, Boundary Layer Concentration Gradients, J. Am. Ceram. Soc. 48 [2], 88-95 (1965).
15. Y. Oishi, Analysis of Ternary Diffusion: Diffusion Equations in Terms of Intrinsic Diffusion Coefficients, submitted to J. Am. Ceram. Soc.
16. Y. Oishi, Analysis of Ternary Diffusion: Solutions of Diffusion Equations and Calculated Concentration Distribution, J. Chem. Phys., in press.
17. Y. Oishi--paper in preparation.
18. J. Crank, Mathematics of Diffusion (Clarendon Press, Oxford, 1956).
19. W. Jost, Diffusion in Solids, Liquids and Gases (Academic Press, New York, 1931).
20. P. G. Shewmon, Diffusion in Solids (McGraw-Hill, New York, 1963).
21. L. Boltzmann, Ann. Physik, 53, 959 (1894).
22. L. S. Darken and R. W. Gurry, The System Iron-Oxygen. II. Equilibrium and Thermodynamics of Liquid Oxide and Other Phases, J. Am. Chem. Soc. 68, 798 (1946).
23. T. Baak and E. J. Hornyak, Jr., The Iron-Oxygen Equilibrium in Glass: Effect of Platinum on the Fe^{2+}/Fe^{3+} Equilibrium, J. Am. Ceram. Soc. 44 [11], 541-44 (1961).
24. J. V. Smith--modifications of K. F. J. Heinreich's table of mass absorption coefficients--unpublished data.
25. G. W. Morey, The Properties of Glass (Reinhold Publishing Corporation, New York, 1938).

26. TRAPSL (A. Z.) Lawrence Radiation Laboratory, Berkeley, Laboratory routine program for calculating diffusivities.

27. P. T. Carter and M. Ibrahim, The Ternary System Na_2O - FeO - SiO_2, J. Soc. Glass Technol. 36, 142-63 (1952); cf. E. M. Levin, C. R. Robbins, and H. F. McMurdie, Phase Diagrams for Ceramists (Am. Ceram. Soc., Columbus, Ohio, 1964).

28. W. A. Weyl, Coloured Glasses (Society of Glass Technology, Sheffield, 1951).

29. N. L. Bowen, J. F. Schairer, and H. W. v. Willems, Am. J. Sci. 5th Ser. 20, 421 (1930); cf. E. M. Levin, C. R. Robbins and H. F. McMurdie, Phase Diagrams for Ceramists, Am. Ceram. Soc., Columbus, Ohio (1964).

30. T. B. King and P. J. Koros, Diffusion in Liquid Silicates, Chapter 12, Kinetics of High Temperature Processes, W. D. Kingery, editor (M. I. T. Technology Press, Cambridge, Mass., 1959).

31. H. Towers and J. Chipman, Diffusion of Calcium and Silicon in a Lime-Alumina-Silica Slag, Trans. A. I. M. E. 203, 769-73; J. Metals (June 1957).

32. W. D. Kingery and J. A. Lecron, Oxygen Mobility in Two Silicate Glasses, Phys. Chem. Glasses, 1 [3], 87-89 (1960).

33. E. L. Williams, Diffusion of Oxygen in Fused Silica, J. Am. Ceram. Soc. 48 [4], 190-194, (1965).

34. J. R. Johnson, R. H. Bristow, and H. H. Blau, Diffusion of Ions in Some Simple Glasses, J. Am. Ceram. Soc. 34 [6], 165-72 (1951).

35. P. LeClerc, Paper VI-5, Fourth International Congress of Glass, Paris, 1956.